Yersinia remodels epigenetic histone modifications in human macrophages

Indra Bekere[1*], Jiabin Huang[1], Marie Schnapp[1], Maren Rudolph[1], Laura Berneking[1], Klaus Ruckdeschel[1], Adam Grundhoff[2], Thomas Günther[2], Nicole Fischer[1], Martin Aepfelbacher[1*]

[1]Institute of Medical Microbiology, Virology and Hygiene, University Medical Center Hamburg-Eppendorf (UKE), Hamburg, Germany

[2] Heinrich-Pette-Institute (HPI), Leibniz Institute for Experimental Virology, Research Group Virus Genomics, Hamburg, Germany

* Corresponding authors

E-mail: ibekere@uke.de (IB), m.aepfelbacher@uke.de (MAe)

Abstract

Various pathogens systematically reprogram gene expression in macrophages, but the underlying mechanisms are largely unknown. We investigated whether the enteropathogen *Yersinia enterocolitica* alters chromatin states to reprogram gene expression in primary human macrophages. Genome-wide chromatin immunoprecipitation (ChIP) seq analyses showed that pathogen-associated molecular patterns (PAMPs) induced up- or down-regulation of histone modifications (HMod) at approximately 14500 loci in promoters and enhancers. Effectors of *Y. enterocolitica* reorganized about half of these dynamic HMod, with the effector YopP being responsible for about half of these modulatory activities. The reorganized HMod were associated with genes involved in immune response and metabolism. Remarkably, the altered HMod also associated with 61 % of all 534 known Rho GTPase pathway genes, revealing a new level in Rho GTPase regulation and a new aspect of bacterial pathogenicity. Changes in HMod were associated to varying degrees with corresponding gene expression, e. g. depending on chromatin localization and cooperation of the HMod. In summary, infection with *Y. enterocolitica* remodels HMod in human macrophages to modulate key gene expression programs of the innate immune response.

Author Summary

Human pathogenic bacteria can affect epigenetic histone modifications to modulate gene expression in host cells. However, a systems biology analysis of this bacterial virulence mechanism in immune cells has not been performed. Here we analyzed genome-wide epigenetic histone modifications and associated gene expression changes in primary human macrophages infected with enteropathogenic *Yersinia enterocolitica*. We demonstrate that

Yersinia virulence factors extensively modulate histone modifications and associated gene expression triggered by the pathogen-associated molecular patterns (PAMPs) of the bacteria. The epigenetically modulated genes are involved in several key pathways of the macrophage immune response, including the Rho GTPase pathway, revealing a novel level of Rho GTPase regulation by a bacterial pathogen. Overall, our findings provide an in-depth view of epigenetic and gene expression changes during host-pathogen interaction and might have further implications for understanding of the innate immune memory in macrophages.

45 # Introduction

46 Macrophages play an essential role in the response to bacterial infection. They sense
47 pathogen-associated molecular patterns (PAMPs) like lipopolysaccharide (LPS), nucleic acids
48 or flagellin through Toll-like, RIG-I-like or NOD-like pattern recognition receptors (PRRs),
49 respectively (Zhang & Mosser, 2008; Takeuchi & Akira, 2010). RIG-I-like and NOD-like PRRs
50 are part of inflammasomes that process and release the major pro-inflammatory cytokines
51 interleukin (IL)-1β and IL-18 (Broz & Dixit, 2016; Lupfer et al., 2015). While PRRs recognize a
52 wide variety of PAMPs, their downstream signaling often converges on mitogen activated
53 protein kinase- (MAPK), nuclear factor κB- (NF-κB) and type I interferon (IFN) signal
54 pathways (Mogensen, 2009; Takeuchi & Akira, 2010). These pathways include activation of
55 transcription factors that control expression of genes for cytokines, chemokines, and
56 inflammasome components, as well as genes for metabolism, cytoskeleton regulation, and
57 transcriptional regulation (Takeuchi & Akira, 2010; Christgen et al., 2020; Ryan & O'Neill,
58 2020; Doyle et al., 2004; Roach et al., 2007). Thousands of functionally diverse genes are up-
59 or downregulated by PAMPs in macrophages. Many of these genes belong to elaborate
60 transcriptional programs that drive macrophage functions during infection. Such programs
61 contribute crucially to the immunological phenomena of priming, tolerance
62 (immunosuppression) and trained immunity (Park et al., 2017; Saeed et al., 2014). The
63 inflammatory gene expression programs in macrophages form an intricate network that is
64 characterized by crosstalk and feedback loops (Park et al., 2017; Kang et al., 2019).
65 Because of their central role in immune defense, numerous pathogenic bacteria have
66 developed mechanisms to suppress or modulate macrophage gene expression (Diacovich &
67 Gorvel, 2010).

68 Pathogenic *Yersinia* species, which comprise the enteropathogens *Y. pseudotuberculosis* and
69 *Y. enterocolitica* as well as the plague agent *Yersinia pestis*, can proliferate extracellularly in
70 lymphoid tissues of animal hosts (Balada-Llasat & Mecsas, 2006; Viboud & Bliska, 2005).
71 Yersiniae can on one hand exploit intracellular niches early during infection, e.g., within
72 macrophages and dendritic cells, in order to disseminate to lymphoid tissues and organs
73 such as spleen and liver (St. John et al., 2014; Spinner et al., 2014; Pujol et al., 2009;
74 Drechsler-Hake et al., 2016; Pujol & Bliska, 2003). On the other hand these bacteria have
75 been shown to suppress phagocytosis, migration and immune signaling in resident cells of
76 the innate immune system (Viboud & Bliska, 2005; Marketon et al., 2005). The major
77 virulence mechanism of pathogenic yersiniae is a type III secretion system (T3SS) by which
78 they inject effector proteins, named *Yersinia* outer proteins (Yops), into immune cells
79 (Cornelis & Wolf-Watz, 1997; Galán & Wolf-Watz 2006; Viboud & Bliska, 2005). The seven
80 known Yops exert different activities to suppress immune cell functions. E.g., YopE, YopT and
81 YopO block cytoskeletal reorganization by modifying the activity of Rho GTP binding proteins
82 (Aktories et al., 2000; Aepfelbacher & Wolters, 2017). Further, YopP/J, and YopM inhibit the
83 inflammatory responses triggered by the PAMPs (e.g., LPS, heptose containing metabolites,
84 T3SS pore or the adhesins YadA and invasin) or the effector-triggered immunity (ETI) elicited
85 by the bacteria (Brodsky et al., 2010; Chung et al., 2016; Mukherjee et al., 2006; Schubert et
86 al., 2020; Auerbuch et al., 2009; Schmid et al., 2004; Grassl et al., 2003; Schulte et al., 2000;
87 Lopes Fischer et al., 2020). Induction of ETI is a consequence of bacterial virulence activities
88 in host cells that disrupt cellular processes and are sensed by the host (Lopes Fischer et al.,
89 2020). *Yersinia* triggers ETI e.g., by the T3SS translocation pore-produced membrane damage
90 or by deactivation of Rho GTPases through YopE and YopT (Schubert et al., 2020). YopP/J
91 acetylates and inhibits components of NF-κB and MAPK pathways and thereby profoundly

92 suppresses pro-inflammatory gene expression downstream of TLRs (Mukherjee et al., 2006).
93 YopM acts by both, increasing production of the anti-inflammatory cytokine IL-10 and
94 counteracting activation of the pyrin inflammasome, which is triggered by the Yop-induced
95 deactivation of Rho GTPases (McPhee et al., 2012; Berneking et al., 2016; Chung et al., 2016).
96 Thus, on one hand pathogenic yersiniae contain immunostimulatory PAMPs and their T3SS
97 effectors elicit ETI that strongly alter gene expression in macrophages. On the other hand,
98 the bacteria employ an arsenal of activities to systematically modulate and antagonize the
99 PAMP- and ETI triggered immune responses (Philip et al., 2016; Schubert et al., 2020; Lopes
100 Fischer et al., 2020).
101 Epigenetic mechanisms play a master role in the regulation of macrophage gene expression.
102 Among others they i) determine the phenotypes of macrophages in different tissues and
103 disease states, ii) control trained innate immunity, iii) regulate priming and immune
104 tolerance and iv) integrate stimulus triggered responses (Ivashkiv, 2013; Park et al., 2017;
105 Glass & Natoli, 2015; Saeed et al., 2014). Gene expression in response to external stimuli is
106 controlled by the concerted activity and binding of macrophage lineage-determining
107 transcription factors and stimulus-regulated transcription factors to accessible cis-regulatory
108 elements (promoters and enhancers) in the cellular chromatin (Ivashkiv, 2013; Glass & Natoli,
109 2015). DNA accessibility is determined by the pre-existing epigenomic landscape, which is
110 the sum of DNA methylation, nucleosome occupancy, pre-bound factors and histone
111 modifications (Klemm et al., 2019). The types of histone modifications located at gene
112 promoters and enhancers influence DNA accessibility and transcriptional activity. For
113 instance, a trimethylated lysine at position 4 in histone 3 (H3K4me3) is characteristic for
114 active promoters, an acetylated lysine at position 27 in histone 3 (H3K27ac) indicates active
115 promoters and enhancers while H3K9me3 signifies repressed, transcriptionally inactive

116 heterochromatin (Rada-Iglesias et al., 2011; Barski et al., 2007; Wang et al., 2008). Most
117 posttranslational histone modifications are transient and their turnover is regulated by
118 enzymes that mediate their deposition or deletion (Yun et al., 2011; Allis & Jenuwein, 2016).
119 Bacterial PAMP-induced signaling has been shown to intensely modulate histone
120 modifications and this has been implicated in priming, immune tolerance and trained
121 immunity in macrophages (Ivashkiv, 2013; Park et al., 2017; Dong & Hamon, 2020; Saeed et
122 al., 2014). Consequently, numerous pathogens can interfere with histone modifications in
123 host cells using unique and sophisticated strategies (Connor et al., 2019; Bierne et al., 2012;
124 Rolando et al., 2013).
125 The current understanding of how *Yersinia* modulates gene expression in macrophages is
126 that it uses its effectors YopP and YopM to interfere with PAMP-induced MAP-kinase and
127 NF-kB signaling to the nucleus (Schubert et al., 2020). Previous microarray or RNA-seq
128 studies of *Yersinia* effects on gene expression were so far conducted in *Y. pestis* infected rat
129 lymph nodes (Comer et al., 2010), African green monkeys (Chakraborty et al., 2019;
130 Hammamieh et al., 2016) and neutrophils (Subrahmanyam et al., 2001), in *Y.*
131 *pseudotuberculosis* infected mouse cecum (Heine et al., 2018) and Peyer's patches (Nuss et
132 al., 2017) as well as in *Y. enterocolitica* infected epithelial and NK cells (Bohn et al., 2004;
133 Koch et al., 2013). In macrophages systematic gene expression analysis was performed
134 during *Y. enterocolitica* or *Y. pseudotuberculosis* infection of cultured mouse macrophages
135 for up to 4 h and utilizing microarrays (Sauvonnet et al., 2002; Hoffmann et al., 2004;
136 Auerbuch et al., 2009; Zhang et al., 2005). Here we employed primary human macrophages
137 and genome wide chromatin immunoprecipitation (ChIP)-seq and RNA-seq technologies to
138 globally analyze histone modifications and associated gene expression patterns for up to 6 h
139 of *Y. enterocolitica* infection. We uncover a profound and coordinated reorganization of

histone modifications as basis for systematic *Yersinia* effects on gene expression in macrophages. In addition to extensive modulation of histone modifications at inflammatory, immune response and metabolism genes, we found that the bacteria caused alterations of histone modifications at 61 % of all 534 known Rho GTPase pathway genes in macrophages. These results describe the previously unrecognized strategy of pathogenic *Yersinia* to modulate specific gene expression programs in innate immune cells through the systematic reorganization of histone modifications.

147 # Results

148 ## Global reorganization of histone modifications in macrophages

149 ## upon *Yersinia enterocolitica* infection

150 We first investigated on a global scale whether *Y. enterocolitica* alters histone modification
151 patterns in human macrophages (Ivashkiv, 2013). For this, *in vitro* differentiated primary
152 human macrophages (S1A Fig) were mock infected or infected with *Y. enterocolitica* wild
153 type strain WA314 or its avirulent derivative WAC and subjected to chromatin
154 immunoprecipitation (ChIP)-seq (Fig 1A). WAC lacks a T3SS and therefore was used to
155 separate the effects of the *Yersinia* PAMPs from the T3SS associated effects (for strains
156 employed in this study see S1 Table). We investigated cells after infection with a multiplicity
157 of infection (MOI) 100 for 6 h, conditions at which 100 % of cells were positive for
158 translocated Yops (S1A Fig) and a maximal effect on gene expression (Berneking et al., 2016)
159 and histone modifications (S1B Fig) but no signs of cell death as measured by membrane
160 permeability (S1C Fig) and caspase-3 cleavage (S1D Fig; Ruckdeschel et al., 1997; Sarhan et
161 al., 2018) are detectable in the human macrophages.

162 ChIP-seq analyzes were performed for four histone-3 (H3) marks whose impact on
163 macrophage gene expression has been well established: H3K4me3, indicating active
164 promoters; H3K4me1, which is highly enriched at distal regulatory elements (enhancers);
165 H3K27ac, indicating active promoters and enhancers; and H3K27me3 indicating inactive
166 promoters and enhancers (Heintzman et al., 2009; Rada-Iglesias et al., 2011; Barski et al.,
167 2007; Wang et al., 2008). Successful ChIP was confirmed using ChIP-qPCR with positive and
168 negative control primers for different histone marks (S2A Fig). Dynamic regions were defined
169 as those exhibiting at least a 2-fold change in any pairwise comparison between mock-,

170 WA314- or WAC infected macrophages. Overall, H3K27ac peaks were the most dynamic (43
171 %) followed by H3K4me3 peaks (7 %), H3K4me1 regions (3 %) and H3K27me3 regions (0.1 %)
172 (Fig 1B). Around half of the dynamic H3K4me3 peaks and H3K4me1 regions and one fourth
173 of the dynamic H3K27ac peaks were at promoters (+/- 2 kb from transcription start site; Fig
174 1C). The remaining half of the dynamic H3K4me3 peaks and H3K4me1 regions and three
175 fourth of the dynamic H3K27ac peaks were at enhancers (H3K4me1-enriched regions
176 outside promoters; Fig 1C).
177 A Spearman correlation heatmap of the H3K27ac peaks and two corresponding datasets
178 published elsewhere from naive and *E. coli* LPS-stimulated primary human macrophages
179 (Park et al., 2017; Novakovic et al., 2016) revealed i) a strong correlation between WAC
180 infected and LPS-treated macrophages (Fig 1D), indicating that the PAMP-induced histone
181 modifications are to a large part caused by LPS, although yersiniae possess a number of
182 additional PAMPs (Reinés et al., 2012; Zhou et al., 2018; Brodsky et al., 2010); ii) a close
183 similarity between the mock-infected macrophages in our study and the naïve macrophages
184 employed in other studies, and iii) a higher similarity of WA314 infected macrophages to
185 naïve and mock-infected macrophages than to WAC- and LPS infected macrophages (Fig 1D).
186 This likely reflects suppression of PAMP/LPS-induced H3K27ac modifications by the T3SS
187 effectors of WA314 (Schubert et al., 2020).
188 We evaluated whether histone marks were significantly (≥ 2-fold change, adjusted P-value ≤
189 0.05) up- or down-regulated in the three pairwise comparisons WAC vs mock, WA314 vs
190 mock and WAC vs WA314 (Fig 1E; S18 Table). An eminent result was that, consistently,
191 around 14-times more H3K27ac regions than H3K4me3 regions were dynamic (Fig 1E; S18
192 Table). Further, 2156 unique H3K4me1 regions were dynamic whereas H3K27me3 regions
193 were essentially unaltered under these conditions (Fig 1E; S18 Table), further suggesting that

194 H3K27me3 marks are not affected by *Yersinia* infection in macrophages. WAC up- and down-
195 regulated histone modifications at 14559 unique loci vs mock, reflecting the effect of the
196 PAMPs (Fig 1E). As determined by comparison with the WAC effects, WA314 inhibited the up
197 regulation of 571 H3K4me3 regions (53 %; Fig 1F) and 2881 H3K27ac regions (42 %; Fig 1G)
198 and inhibited the down regulation of 2627 H3K27ac regions (40 %; Fig 1G).
199 Further analysis revealed that histone modification patterns were modified at promoters of
200 6228 genes and at enhancers of 7730 genes, whereby 2964 genes were modified both at the
201 promoter and nearby enhancer regions (Fig 1H). We conclude that *Y. enterocolitica* triggers
202 extensive reprogramming of chromatin states in human macrophages by regulating
203 H3K27ac-, H3K4me1- and H3K4me3 marks at promoters and enhancers of about 11000
204 genes (Fig 1H).
205
206

207 *Y. enterocolitica* virulence factors suppress PAMP-induced histone
208 modifications at promoters and enhancers

209 We investigated the bacteria induced reprogramming of histone modifications at promoters
210 and enhancers in more detail. By genome wide analysis of dynamic H3K27ac and H3K4me3
211 regions at promoters of mock-, WAC- and WA314 infected macrophages we identified 10
212 clusters which could be assigned to 6 classes and 2 modules (Methods; Fig 2A, S2 Table).
213 Promoter module 1 (P1) contains dynamic H3K4me3- and H3K27ac regions that change
214 concordantly (classes P1a, b; Figs 2A, B). Promoter module 2 (P2) contains dynamic H3K27ac
215 regions at largely constant H3K4me3 regions (classes P2a-d; Figs 2A, B). The patterns of
216 histone modifications in the classes were clearly distinct and assigned to 4 different profiles.
217 In profile “Suppression”, WAC increases deposition of histone marks and this is suppressed

218 by WA314 (P1a and P2a; Figs 2A-C). In profile “Prevention”, WAC downregulates histone
219 marks and this is prevented by WA314 (P1b and P2d; Figs 2A-C). In profile “Down”, WA314
220 selectively downregulates H3K27ac marks when compared to mock and WAC (P2b; Figs 2A-
221 C). In profile “Up” WA314 selectively upregulates H3K27ac marks when compared to mock
222 and WAC (P2c; Figs 2A-C). These profiles are also illustrated by tag densities of H3K4me3 and
223 H3K27ac ChIP-seq at promoters of selected genes (Figs 2C). WA314 strongly counteracted
224 the PAMP-induced up- and downregulation of histone modifications at promoters in
225 Suppression and Prevention profiles, which was also confirmed by ChIP-qPCR analysis of
226 H3K4me3 and H3K27ac for IL6, IL1B and PTGS2 (Suppression) and ASB2 and CEBPE
227 (Prevention) genes (S2B Fig). However, WA314 counter-regulation often was not complete
228 therefore the levels of histone modifications in WA314 infected cells were frequently in
229 between the levels in mock- and WAC infected macrophages (e.g. in Suppression profile
230 classes P1a and P2a; Figs 2A, B).
231 We further sought to investigate in detail the *Yersinia* induced reprogramming of histone
232 modifications at distal regulatory elements/enhancers. A genome wide heatmap of dynamic
233 H3K27ac regions at enhancer regions, characterized by the presence of H3K4me1 marks,
234 was prepared in mock-, WAC- and WA314 infected macrophages (Fig 2D, S3 Table). Six
235 clusters comprising altogether 16408 dynamic enhancers were identified and assembled into
236 four classes (E1-E4; Fig 2D). Analogous to the promoter classes, the enhancer classes E1, E2,
237 E3 and E4 correspond to Suppression, Down, Up and Prevention profiles, respectively (Fig
238 2E). In unstimulated macrophages (mock) enhancers were either poised (no or low level of
239 H3K27ac marks; E1 and E3) or constitutive (presence of H3K27ac marks; E2 and E4) (Figs 2D,
240 E; Ostuni et al., 2010). WAC infection activated poised enhancers by increasing H3K27ac
241 marks (E1) or repressed constitutive enhancers by decreasing H3K27ac marks (E4) (Figs 2D,

242 E). WA314 inhibited the WAC induced up-regulation of poised enhancers in Suppression
243 profile E1 and down-regulation of constitutive enhancers in Prevention profile E4 (Figs 2D, E).
244 WA314 also down-regulated constitutive enhancers in Down profile E2 and up-regulated
245 poised enhancers in Up profile E3 (Figs 2D, E).
246 We also investigated the effect of *Yersinia* on latent enhancers, defined by the initial
247 absence of H3K4me1- and H3K27ac marks (Ostuni et al., 2010). We identified 149 latent
248 enhancers in mock infected macrophages that gained H3K4me1- and H3K27ac marks upon
249 WAC infection, which converts these latent enhancers into a constitutive state (Fig 2F, S4
250 Table). WA314 also increased H3K4me1 levels but did not produce an increase of H3K27ac
251 levels in most of these latent enhancers (Fig 2F). Thus, WA314 infection does not inhibit the
252 unveiling of latent enhancers and their conversion into a poised state by the bacterial
253 PAMPs, but suppresses their transition to a constitutive state.
254 In summary, four profiles describe how *Y. enterocolitica* alters H3K4me3 and H3K27ac marks
255 at macrophage promoters and enhancers. In the profiles Suppression and Prevention, the
256 bacteria's virulence plasmid-encoded factors block the PAMP-induced deposition or removal
257 of H3K4me3- and H3K27ac marks, respectively. In profiles Down and Up the T3SS-associated
258 effectors down- or up-regulate, respectively, H3K27ac marks.
259
260

261 *Yersinia* reorganization of histone marks and gene expression
262 targets central immune pathways in macrophages

263 We asked to what extent the histone modifications reprogrammed by the bacteria associate
264 with expression of the corresponding genes. Therefore, infected macrophages were
265 analyzed by RNA-seq in parallel to ChIP-seq (Fig 1A). 6148 differentially expressed genes

266 (DEGs) were altogether found in three pairwise comparisons (WAC vs mock, WA314 vs mock
267 and WAC vs WA314; Fig 3A; S5 and S6 Tables). Four classes (R1-R4) were identified in the
268 DEGs which corresponded to Suppression- (R1), Down- (R2), Up- (R3) or Prevention (R4)
269 profiles (Fig 3A and S6 Table). WAC up-regulated 3020 genes (Fig 3B) and down-regulated
270 2152 genes (Fig 3C) vs mock reflecting the transcriptional response of macrophages to the
271 PAMPs of *Y. enterocolitica.* In the Suppression profile, 42 % of the genes upregulated by
272 WAC were not or only partly upregulated by WA314 (Fig 3B). In the Prevention profile, 39 %
273 of the genes downregulated by WAC were not or much less downregulated by WA314 (Fig
274 3C). RT-qPCR analysis confirmed WA314 counteraction of PAMP-induced changes in mRNA
275 levels for PPARGC1B (Prevention) and ABI1, IL1B and TNF (Suppression) genes (S2C Fig).
276 WA314 often did not completely reverse the PAMP-induced up- or downregulation of genes,
277 as shown by the fact that gene expression levels in the WA314 infected cells were frequently
278 in between mock- and WAC infected macrophages (e.g. in classes R1 and R4, Fig 3A). Thus,
279 coinciding with histone modifications, gene expression is modulated extensively by *Y.*
280 *enterocolitica* in human macrophages and can also be divided into Suppression-, Down-, Up-,
281 and Prevention profiles.
282 We evaluated all individual histone modifications which associated with gene expression
283 changes in the different profiles and found that Suppression-, Down-, Up- and Prevention
284 profiles showed on average 30 %, 2 %, 4 % and 16 % corresponding gene expression changes,
285 respectively (Fig 3D). Overlap between histone modifications and gene expression was
286 stronger for H3K4me3 and H3K27ac changes at promoters (8-81 % overlap; S3A-C Figs) than
287 for H3K27ac changes at enhancers (5-29 % overlap; S3D Fig), indicating that enhancer
288 modifications associate with direct gene expression to a lesser extent than promoter
289 modifications.

290 To find out whether histone modifications at promoters and enhancers cooperate to
291 regulate gene expression, we analyzed pairwise overlaps of genes associated with promoter-
292 and enhancer classes (Fig 3E). The strongest overlaps occurred in classes belonging to the
293 same profiles: P1a/P2a/E1 (Suppression), P2b/E2 (Down), P2c/E3 (Up) and P1b/P2d/E4
294 (Prevention) (Fig 3E). We found that 57 % of the genes overlapping in the Suppression profile
295 classes and 26 % of the genes overlapping in the Prevention profile classes showed
296 corresponding changes in gene expression (Fig 3F). In comparison, only 4 % and 3 % of genes
297 associated with histone modifications in the Down and Up profile classes, respectively,
298 showed expression changes (Fig 3F). We conclude that reprogramming of histone
299 modifications upon *Y. enterocolitica* infection in macrophages can cause significant changes
300 in gene expression. The size of the effect displays a very wide range from 2 to over 80 % and
301 strongly depends on the localization (promoter or enhancers), cooperation (e.g. at
302 promoters or between related promoters and enhancers) and profile of the histone
303 modifications.
304 To address the question which biological pathways are regulated by the epigenetic
305 reprogramming upon *Yersinia* infection, we subjected all DEGs in the different expression
306 classes/profiles that are associated with histone modifications (Fig 3G) to Gene Ontology
307 (GO) and KEGG analysis (Fig 3H). In profiles Suppression, Down, Up and Prevention, 51 %, 19
308 %, 19 % and 36 % of DEGs, respectively, were associated with at least one corresponding
309 histone modification change (Fig 3G). Thus, the proportion of gene expression changes that
310 is associated with histone modifications is clearly higher than the proportion of histone
311 modifications that is associated with corresponding gene expression changes (compare Fig
312 3D and Fig 3G). Suppression profile genes were most highly enriched in inflammatory
313 response, type I interferon signaling and apoptotic process (Fig 3H) and mainly encode pro-

314 inflammatory cytokines, chemokines, feedback regulators (like TNFAIPs) and type I IFN
315 signaling mediators (Fig 3I, S4A Fig). Down profile was enriched in regulation of transcription
316 (Fig 3H) containing CEBPE and FOS (Fig 3J). CEBPE regulates myeloid lineage differentiation
317 (Bedi et al., 2009), inflammasome activation and interferon signaling (Göös et al., 2019). FOS
318 encoding c-Fos protein is a part of AP1 complex, which regulates macrophage differentiation
319 and long range enhancer interactions (Phanstiel et al., 2017), suppresses pro-inflammatory
320 cytokine and IL-10 expression and increases lysosome mediated bacterial killing (Hop et al.,
321 2018). Up profile genes were enriched in Wnt signaling (Figs 3H, J), which directs
322 macrophage differentiation, regulates expression of key anti-inflammatory mediators and
323 modulates phagocytosis (Malsin et al., 2019). Prevention profile genes were enriched in
324 pathways involving regulation of GTPases, including mostly Rho GTPase pathway genes (Figs
325 3H, K) and in metabolic pathways (Fig 3H), including 22 genes for the metabolism of
326 cholesterol, fatty acids, acyl-CoA or glucose (S7 Table). Suppression profile genes associated
327 with latent enhancers (Fig 2F) were enriched among others in negative regulation of
328 transcription and inflammatory signaling (S4B Fig).
329 Pathogenic *Yersinia* exploit a variety of host signaling pathways for pathogenesis such as
330 MAP kinase (Mukherjee et al., 2006), PI3K/ Akt (Sauvonnet et al., 2002b), cell death (Sarhan
331 et al., 2018) and trafficking pathways, e.g., involving Rab GTPases (Connor et al., 2018).
332 Notably, gene expressions and histone modifications belonging to these pathways are also
333 modulated by *Yersinia* T3SS effectors (Table S16). For instance, *Yersinia* was shown to inhibit
334 activation of the MAPK pathway (Mukherjee et al., 2006) and several MAPK kinases and
335 phosphatases were found to be suppressed by plasmid-encoded virulence factors in the
336 Suppression profile (S4C Fig). Furthermore, both Suppression and Prevention profiles

337 contained genes from Rab GTPase signaling (S4D Fig), which is exploited by pathogenic
338 *Yersinia* to promote intracellular survival (Connor et al., 2018).
339 Analysis of transcription factor (TF) motif enrichment revealed binding sites of inflammatory
340 regulators from the RHD- (NFkB-p65-Rel), IRF- (ISRE, IRF2) and bZIP- (Fra2, Fosl2, Jun-AP1)
341 families in Suppression profile genes (Fig 3J, S4E Fig). No transcription factor motifs were
342 enriched in Down profile. Up profile was enriched for RHD (NFkB-p65-Rel) binding sites (Fig
343 3J, S4E Fig) indicating that *Yersinia* effector activities can lead to increased gene expression
344 also through regulation of NF-κB signaling. Prevention profile genes were enriched for
345 distinct motifs from ETS (SpiB, PU.1) family (Fig 3J, S4E Fig). ETS TFs are known to interact
346 extensively with other TFs (Verger & Duterque-Coquillaud, 2002) and play a role in cytokine
347 gene expression (Gao et al., 2016; Lennard Richard et al., 2014; O'Reilly et al., 2003; Gallant
348 & Gilkeson, 2006) and macrophage differentiation (Glass & Natoli, 2015).
349 Taken together, the histone modifications that are reprogrammed upon *Y. enterocolitica*
350 infection associate with central transcriptional programs in macrophages. Most significantly,
351 PAMP-induced up-regulation of immune signaling and inflammatory response genes is
352 suppressed and the down-regulation of metabolic and Rho GTPase pathway genes is
353 prevented by the bacteria.
354
355

356 *Y. enterocolitica* reprogramms histone marks of Rho GTPase
357 pathway genes

358 Interestingly, the Rho GTPase pathway genes were most significantly enriched in Prevention
359 profile genes connected to histone modifications (Figs 3H, K). It was also found enriched in
360 the Suppression profile and in the latent enhancer associated genes (S8 Table). Altogether,

361 the dynamic histone modifications identified here were associated with 324 unique Rho
362 GTPase pathway genes (61 % of all known Rho GTPase genes; Fig 4A, S9 Table).
363 A great variety of bacterial virulence factors target or imitate Rho proteins or their regulators
364 to manipulate immune cell functions (Heasman & Ridley, 2008; Aktories, 2011). Subversion
365 of Rho GTPase activities is also a central virulence strategy of *Yersinia* and there is mediated
366 by the T3SS effectors YopE, YopT and YopO/YpkA (Aepfelbacher & Wolters, 2017). However,
367 only scarce information is available on the epigenetic regulation of Rho GTPase pathway
368 genes in general and relevant systems-level studies are lacking (Chen et al., 2020).
369 Considering the strong association of dynamic histone modifications with Rho GTPase
370 pathway genes in *Yersinia* infected macrophages, we examined this connection in more
371 detail here.
372 The Rho GTPase family is composed of 20 proteins, which can be divided into 8 subfamilies
373 (Boureux et al., 2006). Rho GTPases are best known for regulating the actin cytoskeleton but
374 also for control of vesicle transport, microtubule dynamics, cell cycle and gene expression
375 (Jaffe & Hall, 2005; Hodge & Ridley, 2016). Through these basic activities, they play central
376 roles in immune cell functions such as phagocytosis, chemotaxis and adhesion (Heasman &
377 Ridley, 2008). The classical Rho GTPases cycle between inactive GDP-bound and active GTP-
378 bound states (Fig 4H). Guanine nucleotide exchange factors (GEFs) promote the dissociation
379 of GDP leading to GTP loading and activation (Laurin & Côté, 2014). Active GTP-bound Rho
380 proteins stimulate effector proteins which carry out basic molecular activities (Bagci et al.,
381 2020; Mott & Owen, 2015). GTPase activating proteins (GAPs) bind to GTP-loaded Rho
382 proteins and thereby stimulate their intrinsic GTPase activity and lead to their deactivation
383 (Tcherkezian & Lamarche-Vane, 2007). Most GEFs, GAPs and effectors are not specific for
384 individual Rho GTPases but associate with members of one or more subfamilies (Müller et al.,

385 2020; Bagci et al., 2020). Currently 77 RhoGEFs (Laurin & Côté, 2014), 66 Rho GAPs
386 (Tcherkezian & Lamarche-Vane, 2007) and up to 370 Rho GTPase effectors are known,
387 whereby the number of effectors may still be growing (Bustelo et al., 2007; Paul et al., 2017;
388 Bagci et al., 2020).
389 Notably, 68 %, 62 %, 58 % and 74 % of all known genes for GAPs, GEFs, effectors and Rho
390 proteins, respectively, exhibited altered histone modification patterns in *Y. enterocolitica*
391 infected macrophages (S5A Fig "RNA & ChIP" and "ChIP only" fractions). Histone
392 modifications were concomitantly altered at enhancers and promoters of 127 Rho GTPase
393 pathway genes (S5B Fig). More than 2 enhancer regions in the E1 and E4 enhancer classes
394 were on average associated with an individual Rho GTPase pathway gene (Fig 4A) and the
395 number of enhancers per Rho GTPase gene ranged from 1 to 14 (S5C Fig, S9 Table). FNBP1,
396 RAPGEF1 and ELMO1 were the genes for which 13, 13 and 14 putative enhancers,
397 respectively, were found (S9 Table).
398 To draw the most informed conclusion about the biological significance of Rho GTPase
399 pathway gene regulation by *Yersinia*, we created a heatmap of all Rho GTPase pathway DEGs
400 in mock-, WAC-, and WA314-infected macrophages independent of their association with
401 histone modifications (Bustelo et al., 2007; Paul et al., 2017; Bagci et al., 2020; Müller et al.,
402 2020; Wennerberg et al., 2004; Senoo et al., 2019). This revealed altogether 204 DEGs in
403 Suppression-, Down-, Up- and Prevention profiles (classes R1-R4, Fig 4B, S10 Table). Of these,
404 29 encode GTPase activating proteins (GAPs), 31 guanine nucleotide exchange factors (GEFs),
405 134 effectors and 11 Rho GTPases (S10 Table). 115 (56 %) of these DEGs were in fact
406 associated with dynamic histone modifications (Fig 4C).
407 Recently all known proteins with putative GAP or GEF activities were biochemically
408 characterized regarding their actual effect on the three main Rho family proteins RhoA, Rac1

409 and Cdc42 (Müller et al., 2020). Analysis of our data in view of this report revealed that in
410 the Prevention profile 60 % of the active GAPs (6/10) act specifically on Rac as compared to
411 36 % (18/50) of all known GAPs (Figs 4D, E, S11 Table; Müller et al., 2020). In the Suppression
412 profile, Rho-, Rac- or Cdc42 specific GAP genes are not enriched and the percentages of GAP
413 activities acting on Rho (25 %) or Rac (25 %) are identical to those of total GAPs (Figs 4D, E;
414 Müller et al., 2020). We conclude that aided by epigenetic remodelling *Y. enterocolitica*
415 tends to keep Rac-inhibiting GAPs at the level of uninfected cells.
416 Of the 8 Rho GTPase genes in the Suppression and Prevention profiles, three encode
417 classical Rho proteins (Rac1, RhoC, RhoG) and five encode atypical Rho proteins (RhoH, RhoU,
418 RND1, RhoBTB1, RhoBTB2) (Fig 4F). Most atypical Rho proteins are considered constitutively
419 active and consequently are not regulated by GEFs and GAPs but instead are controlled at
420 the level of transcription and targeted destruction, i.e. proteasomal degradation
421 (Aspenström et al., 2007; Haga & Ridley, 2016). The cellular levels of RhoC and RhoG were
422 also shown to be transcriptionally regulated (Vincent et al., 1992; Fritz et al., 1999). Classical
423 and atypical Rho proteins often have overlapping cellular functions and share the same
424 effector proteins. Atypical Rho proteins have so far been implicated in multiple activities
425 including tumour suppression (e.g. RhoBTB2), cell transformation and -morphogenesis as
426 well as development (e.g. RhoU and Rnd) (Aspenström et al., 2007; Stiegler & Boggon, 2020;
427 Hodge & Ridley, 2016; Chardin, 2006). Many atypical Rho proteins have been found to
428 regulate the activity of classical Rho Proteins, e.g. RhoH spatially controls Rac1 activity
429 (Tajadura-Ortega et al., 2018) and Rnd proteins bind and steer Rho GAP proteins to specific
430 cell sites (Stiegler & Boggon, 2020). Notably, the Rho protein genes in the Suppression
431 profile include Rac1, the Rac1 activator RhoG and the atypical Rho proteins RhoH and RhoU
432 (Fig 4F). These Rho proteins can alternatively activate Rac effectors, spatiotemporally control

433 Rac activity or take over Rac functions in cells (Bagci et al., 2020; Aspenström et al., 2007;
434 Hodge & Ridley, 2016; Tajadura-Ortega et al.,2018; Chardin, 2006). Thus, a prominent effect
435 of *Yersinia* in the Suppression profile is to inhibit the expression of genes, whose products
436 can keep up Rac activity. This effect complements well the blocked downregulation of Rac
437 GAPs in the Prevention profile (Figs 4D, E).
438 Altogether epigenetically controlled gene expression might cause low Rac activity in *Yersinia*
439 infected cells and thereby cooperate with the Rac down-regulating T3SS effectors YopE,
440 YopO and YopT (Aepfelbacher & Wolters, 2017).
441 66 Rho GTPase effectors were altogether found in the overlaps of gene expression and
442 epigenetic profiles (S5A, D, F Figs; Bustelo et al., 2007; Paul et al., 2017; Bagci et al., 2020).
443 This includes effectors for all eight Rho GTPase subfamilies (Rho, Rac, Cdc42, RhoD/Rif, Rnd,
444 Wrch-1/Chp, RhoH and RhoBTB) (S5F Fig, S12 Table). Interestingly, while *Yersinia* prevents
445 downregulation of genes for the atypical RhoBTBs (Fig 4F), it at the same time suppresses
446 expression of genes encoding specific RhoBTB effectors (S5F Fig, S12 Table). Furthermore, 19
447 of the identified Rho GTPase effectors have been implicated in epigenetic and transcriptional
448 regulation, suggesting mechanisms for crosstalk and feedback in the epigenetic control of
449 Rho GTPase pathway gene expression (S12 Table). Another level of regulation is provided by
450 the finding that some DEGs from Suppression- and Prevention profile genes belong to the
451 machinery for ubiquitination and/or proteasomal degradation of Rho proteins (Fig 4G;
452 Hodge & Ridley, 2016).
453 Altogether these data indicate that yersiniae modulate expression of a large part of Rho
454 GTPase pathway genes in macrophages through reprogramming of cellular chromatin on
455 multiple levels (S5D, E Figs, Figs 4E, F, H).
456

457 **YopP is a major modulator of epigenetic reprogramming upon *Y.***

458 ***enterocolitica* infection**

459 The *Y. enterocolitica* T3SS effectors YopP (YopJ in *Y. pseudotuberculosis*) and YopM have
460 been shown to modulate inflammatory gene expression in *Yersinia* infected macrophages
461 (Schubert et al., 2020). We therefore examined whether YopP and YopM contribute to the
462 epigenetic reprogramming by *Y. enterocolitica.* Macrophages were infected (6 h) with
463 WA314 strains lacking YopP or YopM (strains WA314ΔYopP or WA314ΔYopM; S1 Table) and
464 investigated using ChIP-seq and RNA-seq (H3K4me3 and H3K27ac modifications; Fig 1A).
465 Principal component analysis (PCA) revealed that the WA314ΔYopM- and WA314 induced
466 H3K27ac- and H3K4me3 modifications located close to each other, while the WA314ΔYopP
467 induced modifications were clearly separate (Fig 5A, S6A Fig). This suggests that YopP but
468 not YopM significantly contributes to the epigenetic changes produced by WA314. The
469 effects of WA314ΔYopP and WA314ΔYopM were directly compared with the effects of
470 WA314 on H3K27ac- and H3K4me3 modifications and gene expression. Notably, 684
471 H3K4me3 regions and 5094 H3K27ac regions were differentially regulated between
472 WA314ΔYopP and WA314 (Fig 5B). In contrast, altogether only 29 histone modifications
473 were differentially regulated between WA314ΔYopM and WA314 (Fig 5B). While 1616 DEGs
474 were detected between WA314ΔYopP and WA314, also 804 DEGs were found between
475 WA314ΔYopM and WA314 (Fig 5B). This suggests that YopP affects gene transcription in
476 macrophages to a large extent through modulation of H3K27ac- and H3K4me3 histone
477 modifications. In contrast, although YopM strongly affects gene transcription, it does not do
478 so by regulating H3K4me3- and H3K27ac histone modifications. We next studied what
479 proportions of the WA314-induced histone modifications in the Suppression-, Prevention-,
480 and Up- and Down profiles were due to YopP (S6B Fig). For this, the percentage YopP effect

481 was calculated from the ratio of fold change (FC) between WA314ΔYopP vs WA314 and
482 either WA314 vs WAC (Suppression and Prevention profiles) or WA314 vs mock (Up and
483 Down profiles). In the promoter and enhancer classes the median Yop contribution to the
484 WA314 effects was 42 % and ranged from 8.9 % - 57.2 % (S6B Fig). Furthermore, the median
485 YopP contribution to the WA314 effects on gene expression associated with histone
486 modifications was 51.4 % (S6C Fig). We conclude that YopP on average contributes around
487 one half to the effects of *Y. enterocolitica* on histone modifications and gene expression.
488 Consequently, other T3SS associated virulence factors - except YopM – also contribute
489 significantly.
490 We looked in more detail at the effects of YopP on Rho GTPase pathway genes (Fig 4, S13
491 Table). In the Suppression- and Prevention profiles of Rho GTPase pathway genes, YopP
492 contributed in the mean 48.5 % and 78.5 %, respectively, to the WA314 effects on gene
493 expression (S13 Table). However, at the level of individual genes the YopP effect was widely
494 spread from 2 to 103 % in the Suppression- and from 29 to 177 % in Prevention profile (Fig
495 5C, S13 Table). We tested whether this widely distributed effect of YopP also applies to
496 inflammatory genes (Fig 3H, S4A Fig, S14 Table). Notably, while the mean effect of YopP on
497 the Suppression profile inflammatory genes was 46 % (S14 Table), the effect on individual
498 genes was spread from -57 to 103 % (Fig 5D). Although the majority of YopP induced
499 changes in gene expression were associated with corresponding YopP induced changes in
500 histone modifications, some YopP regulated genes were associated with histone
501 modifications induced by other T3SS effectors and vice versa (e.g. IL2RA highlighted in Figs
502 5D, E; S13 and S14 Tables, S6D Fig). Further, although YopP contribution to gene expression
503 and histone modifications was evident for the majority of genes and regions associated with
504 inflammatory response and Rho GTPase pathways, the YopP effects on gene expression on

505 one hand and histone modifications on the other hand frequently did not correlate (S6D Fig).
506 Thus, the YopP effect on the expression of individual Rho GTPase pathway and inflammatory
507 genes varies considerably from representing the complete *Yersinia* wild type effect to just a
508 minor contribution. It thereby appears that different T3SS effectors and histone
509 modifications contribute to the widely varying YopP effects on gene expression.
510 YopP/YopJ blocks PAMP-induced inflammatory gene expression by inhibiting NF-κB and
511 MAP-kinase signaling (Schubert et al., 2020). Interestingly, MAP-kinases also phosphorylate
512 histone-3 at serine-10, a modification that is thought to promote the deposition of activating
513 histone marks like H3K14ac and H3K16ac (Sawicka & Seiser, 2014). We therefore sought to
514 find out whether YopP reduces the deposition of H3K4me3- and/or H3K27ac marks through
515 inhibition of MAP-kinases. WA314 inhibited the deposition of H3K4me3 at the IDO1- and
516 SOCS3 promoters and deposition of H3K27ac at the SOCS3 and PTGS2 promoters in the
517 macrophages (Fig 5F). YopP contributed to the WA314 effects on these genes, as seen by
518 significantly less inhibitory activity of WA314ΔYopP on deposition of the histone marks when
519 compared to WA314 (Fig 5F). When combined with the MAP-kinase inhibitors SB203580 and
520 PD98059, targeting p38 and MEK1, respectively, WA314ΔYopP was nearly as effective as
521 WA314 in inhibiting the deposition of H3K4me3 marks at the IDO1 and SOCS3 promoters
522 and deposition of H3K27ac marks at the PTGS2 and SOCS3 promoters (Fig 5F). Thus, MAP-
523 kinase inhibitors can substitute for the missing YopP activity in WA314ΔYopP. This is
524 consistent with the idea that YopP blocks deposition of the histone marks through MAP-
525 kinase inhibition.
526 Finally, we wanted to determine whether the histone modification-driven reprogramming of
527 Rho GTPase pathway genes has functional consequences in macrophages. For this, we took
528 advantage of suppression of ABI1 gene expression by WA314, which is entirely dependent

529 on YopP (Fig 5C and S6D Fig). ABI1 encodes a component of the WAVE regulatory complex
530 that controls actin polymerization in macrophages (Chen et al., 2014; Stahnke et al., 2021).
531 ChIP-qPCR analysis confirmed that YopP suppresses H3K27ac at enhancer within ABI1 gene
532 and H3K4me3 at ABI1 promoter (S6E Fig). Interestingly, during WA314ΔYopP infection
533 treatment with MAP kinase inhibitors suppressed only H3K4me3 and not H3K27ac (S6E Fig),
534 suggesting that different signaling pathways regulate promoter H3K4me3 and enhancer
535 H3K27ac. Gene expression analysis by RT-qPCR confirmed suppression of ABI1 expression by
536 YopP, which was dependent on inhibition of the MAPK pathway (S6F Fig). Corresponding to
537 gene expression, the ABI1 protein was upregulated in WA314ΔYopP- compared to WA314
538 infected macrophages and this could be prevented by MAP-kinase inhibitors (Fig 5G). In the
539 WA314ΔYopP infected macrophages ABI1 prominently accumulated at cell cell contacts,
540 where it colocalized with actin, vinculin and the zonula occludens protein ZO1 (Figs 5H, I).
541 Further, accumulation of ABI1 was associated with increased levels of actin at the cell cell
542 contacts, indicating enhanced WAVE regulatory complex-induced actin polymerization (Figs
543 5H, I; Yamazaki et al., 2007). Notably, accumulation of ABI1 and actin was reversed by
544 treatment of p300 histone acetyltransferase inhibitor C646 (Fig 5J; S6G Fig). Altogether this
545 data shows that through inhibition of the MAPK pathway YopP targets histone modifications
546 and gene expression of the ABI1 gene, causing a redistribution of ABI1 and actin in *Yersinia*
547 infected macrophages.
548
549
550
551

552 # Discussion

553 At present only scarce information is available on epigenetic reprogramming of immune cells
554 by pathogenic bacteria (Rolando et al., 2013; Pacis et al., 2019). This study was conducted to
555 find out whether the enteropathogen *Y. enterocolitica* alters chromatin states to globally
556 control gene expression in human macrophages. Our results provide a number of novel
557 insights into systemic reorganization of epigenetic histone modifications in human
558 macrophages upon infection of pathogenic yersiniae.

559 A primary goal was to map in detail whether and how the effects of the *Yersinia* PAMPs on
560 histone modifications are reorganized by the T3SS associated virulence factors of the
561 bacteria. To this end, we systematically compared the effects of a *Y. enterocolitica* wild type
562 strain and a derived avirulent strain.

563 Infection with virulent and avirulent yersiniae extensively reorganized histone marks
564 (H3K4me1, H3K4me3 and H3K27ac) at macrophage gene promoters and enhancers.
565 H3K27ac marks were the most dynamic (> 22.000 loci altered) followed by H3K4me1 marks
566 (2156 loci altered). That H3K27ac marks are highly dynamic in human macrophages
567 stimulated with bacterial agents has been reported previously (Novakovic et al., 2016).

568 We could classify the bacteria-induced reorganization of histone modifications into four
569 profiles, which we named Suppression, Down, Up and Prevention. In the Suppression- and
570 Prevention profiles, the bacteria's T3SS effectors block the PAMP-induced deposition or
571 removal, respectively, of histone marks. In Down- and Up profiles, the T3SS-associated
572 effectors down- or up-regulate, respectively, histone marks independently of PAMP
573 activities.

574 The fraction of histone modifications overlapping with actual gene expression in the four
575 profiles varied widely. Overlaps ranged from 30 % in the Suppression profile to 2% in the

576 Down profile. The biological significance of *Yersinia*-modulated histone modifications that do
577 not immediately affect gene expression is unclear. It has been observed that chromatin
578 changes in stimulated macrophages do not always associate with gene expression (Park et
579 al., 2017; Qiao et al., 2013; Kang et al., 2019). These "silent" histone modifications may be
580 involved in priming, immune memory, immune tolerance or other complex gene regulatory
581 processes in macrophages (Glass & Natoli, 2015; Ivashkiv, 2013).
582 It was interesting to note that different histone marks at individual promoters or at related
583 promoters and enhancers were reorganized in a coordinated manner upon infection, mostly
584 in the Suppression- and Prevention profiles. In these instances, the histone modifications
585 were more frequently associated with changes in gene expression. Thus, the activity of
586 bacterial pathogenicity factors lead to systematic co-regulation of different histone
587 modifications to effectively act on gene transcription.
588 The T3SS effector YopP accounted for 40-50% of the changes in histone modifications and
589 gene expression produced by virulent *Y. enterocolitica* in macrophages, as exemplified with
590 inflammatory and Rho GTPase pathway genes. Inhibition of MAP-kinase signaling was a
591 crucial mechanism underlying these YopP effects for selected target genes. YopP regulated
592 the expression of genes, at which it changed histone modifications, to very different degrees.
593 E.g., for individual inflammatory or Rho GTPase pathway genes the contribution of YopP to
594 the *Yersinia* effect ranged from null to 100%. Interestingly, the histone modifications at
595 some of the genes whose expression was strongly affected by YopP were changed by other
596 T3SS effectors. We could exclude YopM as one of these effectors, because it did not alter
597 close to any of the histone modifications investigated here. Thus, YopP but not YopM
598 regulates the expression of selective genes through histone modifications and thereby
599 seemingly cooperates to varying extents with other T3SS effectors. Of note, in addition to

600 histone modifications, other gene regulatory mechanisms clearly also contribute to the
601 *Yersinia*- and YopP effects on gene expression (Köberle et al., 2012). Thus, our data suggest
602 that virulent yersiniae fine tune expression of individual genes in specific biological pathways
603 through governing the cooperation between histone modifications and other gene
604 regulatory mechanisms. For this the bacteria employ YopP as the main T3SS effector that
605 cooperates with other effectors. Together the effectors mostly remodel PAMP-induced
606 signal transduction but also exert PAMP independent effects on gene transcription (Köberle
607 et al., 2012).
608 Among the most significant findings of our study was the remodeling of histone
609 modifications at 61 % of all 534 known Rho GTPase genes. When considered in terms of
610 gene expression, 38 % of all known Rho GTPase pathway genes were differentially expressed
611 whereby well over half of them were associated with dynamic histone modifications. The
612 latter encode Rho proteins (Rho GTPases) and their effectors, activators (GEFs) and
613 deactivators (GAPs). To control dynamic cellular processes such as cytoskeletal
614 reorganization or vesicular transport, the right Rho proteins, regulators and effectors have to
615 be activated or deactivated at the right time and location. Rho GTPase signaling networks
616 are characterized by the sheer countless interactions that can take place between the
617 different Rho GTPases, regulators and effectors and by crosstalk and feedback loops (Bustelo
618 et al., 2007; Paul et al., 2017; Bagci et al., 2020; Müller et al., 2020). Our results add a further
619 level of complexity to Rho GTPase regulation in macrophages by revealing an extensive
620 epigenetic control of Rho GTPase pathway gene expression.
621 One of our intriguing findings was that genes encoding GAPs for Rac were overrepresented
622 in the Prevention profile. This indicates that epigenetic changes upon *Yersinia* infection
623 create a cellular state in which downregulation of Rac inhibitors is prevented, which favours

624 Rac inhibition. Inhibition of Rac is a known central strategy of *Yersinia* with the three T3SS
625 effectors YopE, YopT and YopO acting as Rac inhibitors (Aepfelbacher & Wolters, 2017).
626 Further consistent with this bacterial strategy is the finding that expression of Rac1, the Rac1
627 activator RhoG and the atypical Rho proteins RhoH and RhoU, which can take over Rac
628 functions (Bagci et al., 2020; Aspenström et al., 2007; Hodge & Ridley, 2016; Tajadura-
629 Ortega et al.,2018; Chardin, 2006), were suppressed by the bacteria . A reason why *Yersinia*
630 places a focus on inhibition of Rac may be the outstanding role that it plays in anti-microbial
631 activities of macrophages such as phagocytosis, chemotaxis and production of reactive
632 oxygen species (Bokoch, 2005). Rac inhibition by YopE also prevents overshooting
633 translocation of T3SS effectors into cells (Aepfelbacher & Wolters, 2017). A number of genes
634 for atypical Rho proteins (RHOH, RHOU, RND1, RHOBTB1, RHOBTB2) were found in the
635 Suppression and Prevention profiles. The activities of atypical Rho proteins are generally
636 controlled by gene transcription and protein degradation and not by GAPs and GEFs
637 (Aspenström et al., 2007; Haga & Ridley, 2016), but their regulation by epigenetic
638 mechanisms has so far not been reported. Although the specific functions of atypical Rho
639 proteins in macrophages are widely unknown, atypical Rho proteins also can regulate the
640 activity of classical Rho proteins in different cell types (Aspenström et al., 2007; Stiegler &
641 Boggon, 2020; Hodge & Ridley, 2016; Chardin, 2006). For instance, RhoH spatially controls
642 Rac1 activity (Tajadura-Ortega et al.,2018) and Rnd proteins bind and steer Rho GAP proteins
643 to specific cell sites (Stiegler & Boggon, 2020). We also found that downregulation of genes
644 for the atypical Rho proteins RhoBTBs was prevented and expression of genes for some
645 RhoBTB effectors was suppressed in parallel by the bacteria. Thus, through epigenetic
646 mechanisms *Yersinia* may determine which atypical Rho protein/effector pairs are functional
647 in macrophages. Considering the universal role that Rho GTPases play in cellular function,

648 the multifaceted epigenetic regulation of their expression will undoubtedly affect their
649 activities and thereby have functional consequences in macrophages.
650 Providing support for this notion, we here show that MAP kinase (MAPK) pathway regulates
651 histone modifications, gene expression and protein levels of ABI1 gene with associated
652 redistribution of actin cytoskeleton and ABI1 protein, a component of the WAVE actin
653 regulatory complex, at macrophage-macrophage contacts. Furthermore, treatment of
654 macrophages with p300 histone acetyltransferase inhibitor reversed this ABI1 and actin
655 accumulation, providing a direct link between histone modifications and actin reorganization.
656 Increased ABI1 enhances actin accumulation and recruitment of adhesion proteins at these
657 contacts, likely promoting the stabilization of these structures (Ryu et al., 2009; Zipfel et al.,
658 2006).
659 Taken together, in this study we decipher key principles of epigenetic reorganization of
660 human macrophages upon infection of the bacterial enteropathogen *Y. enterocolitica*. 1)
661 Remodeling of histone modifications and associated changes in gene expression can be
662 classified in different profiles, with virulent bacteria mainly suppressing or preventing the
663 effects of bacterial PAMPs, but also exerting independent stimulatory or inhibitory activities
664 through their T3SS effectors. Suppressed histone modifications with corresponding gene
665 suppression mostly belong to immune and inflammatory signaling, whereas prevented
666 modifications/genes belong to Rho GTPase pathway and metabolic pathways (Fig 6). 2)
667 Changes in the different histone modifications at promoters and enhancers are often
668 coordinated, so that they can act cooperatively on gene expression. 3) The T3SS effector
669 YopP contributes up to 50 % to *Yersinia*-induced remodeling of histone modifications and
670 gene expression, through its inhibitory effect on MAP kinase signaling. At the level of
671 individual gene expression, the contribution of YopP varies from null to 100%, even in genes

672 belonging to the same biological pathways. 4) Histone modifications, transcription factor
673 expression, and other unidentified mechanisms are reprogrammed by YopP and other T3SS
674 effectors and cooperatively cause the effects of *Yersinia* on individual gene expression. 5)
675 While there was an up to 30% overlap between histone modifications and associated gene
676 expression in the profiles, the majority of histone modifications did not alter gene
677 expression. In these cases, such epigenetic modifications could prepare cells for subsequent
678 stimuli or provide a basis for innate immune memory or tolerance. Further studies are
679 warranted to test these intriguing possibilities.
680
681
682

683 # Materials and Methods

684 ## Bacterial strains

685 *Yersinia enterocolitica* strains used in this study are derivatives of the serotype O:8 strain
686 WA314 harboring the virulence plasmid pYVO8 (Heesemann & Laufs, 1983). WA314ΔYopM
687 was constructed by replacing the YopM gene in WA314 with a kanamycin resistance cassette
688 (Trülzsch et al., 2004). WA314ΔYopP was generated by insertional inactivation of *yopP* gene
689 (Ruckdeschel et al., 2001). WA314-YopE-ALFA strain was constructed using CRISPR-Cas12a-
690 assisted recombineering approach as described in preprint from Carsten et al., 2021. S1
691 Table provides an overview of the bacterial strains used in this study and oligonucleotide
692 sequences for the generation of WA314-YopE-ALFA strain.

693

694 ## Cell culture

695 Human peripheral blood monocytes were isolated from buffy coats as described in Kopp et
696 al., 2006. Cells were cultured in RPMI1640 containing 20 % autologous serum at 37 °C and 5
697 % CO_2 atmosphere. The medium was changed every three days until cells were
698 differentiated into macrophages after 7 days. Macrophages were used for infection 1 week
699 after the isolation except for RNA-seq experiments for two mock, WA314 and WA314ΔYopM
700 samples from Berneking et al., 2016 and WA314ΔYopP RNA-seq samples where cells were
701 used after 2 weeks of differentiation (RNA-seq samples from batch 2 in S17 Table).

702

703 ## Infection of cells

704 On the day before infection of primary human macrophages the cell medium was changed
705 to RPMI1640 without antibiotics and serum and precultures of *Y. enterocolitica* strains (S1

706 Table) were grown overnight in LB medium with appropriate antibiotics at 27 °C and 200 x
707 rpm. On the day of infection precultures were diluted 1:20 in fresh LB medium without
708 antibiotics and incubated for 90 min at 37 °C and 200 x rpm to induce activation of the
709 *Yersinia* T3SS machinery and Yop expression. Afterwards bacteria were pelleted by
710 centrifugation for 10 min at 6000 x g, 4 °C and resuspended in 1 ml ice-cold PBS containing 1
711 mM $MgCl_2$ and $CaCl_2$. The optical density OD_{600} was adjusted to 3.6 and afterwards
712 macrophages were infected at multiplicity-of-infection (MOI) of 100. Cell culture dishes were
713 centrifuged for 2 min at RT and 200 x g to sediment bacteria on the cells and synchronize
714 infection. Cells were incubated at 37 °C for 6 h.
715

716 **CFU assay**

717 For analysis of bacterial growth (S1E Fig) *Yersinia* cultures were prepared and cells infected
718 as described above in "Infection of cells". Bacterial sample at 0 h was prepared from bacteria
719 used as an input. Afterwards macrophages and bacteria present in the wells were harvested
720 by scraping without washing and centrifuged at 5000 x g at 4 °C. Pellet was resuspended in
721 0.5 % Digitonin in PBS to lyze macrophages and not bacteria and incubated for 10 min on ice.
722 Afterwards lysate was used to prepare 10-fold serial dilutions, which were plated in
723 duplicate on LB agar plates containing appropriate antibiotics. Plates were incubated at 26
724 °C for 24 h before counting the colonies. Two independent experiments with different
725 biological replicates were used for the analysis. The results showed that the number of wild
726 type *Yersinia* at 6 h increased about 3 fold when compared to 0 h (S1E Fig) indicating a low
727 level of replication under selected infection conditions.
728
729

730 ## SYTOX Green assay

731 For analysis of cell death during infection SYTOX Green assay (Thermo Fisher Scientific) was
732 performed which measures membrane permeability (Grootjans et al., 2016). $6x10^4$
733 macrophages per well in a 96-well plate were seeded in RPMI1640 on the day before
734 analysis. The following day macrophages were treated with PBS (mock), WA314 (MOI 100)
735 or positive control (1 % TRITON-X-100) in duplicates. Plates were centrifuged for 2 min at RT,
736 200 x g and incubated at 37 °C for 6 h. SYTOX Green reagent was added to cells 30 min
737 before the end of 6 h incubation. SYTOX fluorescence due to membrane permeabilization
738 was measured with plate reader (Tecan infinite M200) at 485/520 nm. Two biological
739 replicates were used for the analysis.

740

741 ## Flow cytometry

742 Antibody staining for flow cytometry was done in FACS buffer (PBS, 0.1 % BSA) at room
743 temperature in the dark for 30 min, followed by washing in FACS buffer and fixation with 2 %
744 paraformaldehyde in FACS buffer. Cells were stained with the following antibodies: anti-
745 CD14 (Biolegend, 301806), anti-CD16 (Biolegend, 302018), anti-CD38 (Biolegend, 301806),
746 anti-CD86 (BD biosciences), anti-HLA-DR (Biolegend, 307642), anti-CD163 (Biolegend,
747 333608) and anti-CD206 (Biolegend, 321109). In addition, cells were stained with live/dead
748 dye (Invitrogen, P30253) to identify live cells.
749 Flow cytometry data was acquired on a Celesta flow cytometer (BD biosciences) and flow
750 cytometry data was analyzed using Flowing software (Turku Bioscience). Analysis showed
751 that 63.9 % of macrophage culture were $CD14^+$ macrophages (S1F Fig). $CD14^+$ macrophages
752 were positive for macrophage markers CD38 (99 %), CD86 (98.5 %), HLA-DR (74.9 %), CD206
753 (91.6 %), CD163 (61.6 %) and CD16 (88 %) (S1F Fig).

754 ## Treatment with inhibitors

755 For the MAPK pathway inhibition combination of 5 µM SB203580 (Cayman Chemical) and 5
756 µM PD98059 (Merck Millipore), which target p38 and MEK1, respectively, was used.
757 Inhibitors were added to macrophages 30-60 min before the infection.
758 Staurosporine (LC Laboratories; 5 µM) or C646 (Merck; 10 µM) were added at the start of
759 infection.
760

761 ## RNA-seq

762 Total RNA of 1-2 x 10^6 human macrophages (2-4 biological replicates/ macrophage donors
763 per condition, see Table S17) was isolated using RNeasy extraction kit (Qiagen) including
764 DNAse treatment according to manufacturer's instructions. RNA integrity of the isolated
765 RNA was analyzed with the RNA 6000 Nano Chip (Agilent Technologies) on an Agilent 2100
766 Bioanalyzer (Agilent Technologies). mRNA was extracted using the NEBNext Poly(A) mRNA
767 Magnetic Isolation module (New England Biolabs) and RNA-seq libraries were generated
768 using the NEBNext Ultra RNA Library Prep Kit for Illumina (New England Biolabs) as per
769 manufacturer's recommendations. Concentrations of all samples were measured with a
770 Qubit 2.0 Fluorometer (Thermo Fisher Scientific) and fragment lengths distribution of the
771 final libraries was analyzed with the DNA High Sensitivity Chip (Agilent Technologies) on an
772 Agilent 2100 Bioanalyzer (Agilent Technologies). All samples were normalized to 2 nM and
773 pooled equimolar. The library pool was sequenced on the NextSeq500 (Illumina) with 1 x 75
774 bp and total 19.9 to 23.8 million reads per sample.
775
776

RNA-seq analysis

Sequencing reads containing bases with low quality scores (quality Phred score cutoff 20) or adapters were trimmed using TrimGalore program (http://www.bioinformatics.babraham.ac.uk/projects/trim_galore/).

Reads were aligned to the human reference assembly hg19 using STAR (Dobin et al., 2012). FeatureCounts (Liao et al., 2014) was employed to obtain the number of reads mapping to each gene.

RNA-seq data have been deposited in the ArrayExpress database at EMBL-EBI (www.ebi.ac.uk/arrayexpress) under accession number E-MTAB-10473. RNA-seq data from additional replicates of mock, WA314 6h and WA314ΔYopM 6h were obtained from European Nucleotide Archive (ENA) at http://www.ebi.ac.uk/ena/data/view/PRJEB10086.

RNA-seq differential expression analysis

Statistical analysis of differential expression was carried out with DESeq2 (Love et al., 2014) using raw counts as an input and the experimental design *~batch + condition*. Significantly enriched genes were defined with fold change ≥ 2 and adjusted P-value ≤ 0.05. Normalized rlog counts for each gene were obtained after batch effect removal with limma package (Ritchie et al., 2015) and used for downstream clustering analysis and visualization. PCA analysis and sample distance heatmaps confirmed high reproducibility between all biological replicates (see Table S17) used in the analysis.

Clustering analysis of all DEGs from comparisons between mock, WAC, WA314 was done with rlog counts in R with pheatmap package. Clustering was performed with clustering distance based on Euclidean distance and Complete clustering method to yield 6 clusters

801 which were further assembled into profiles Suppression, Prevention, Up and Down.
802 Clustering distance, clustering method and number of clusters were selected so that all
803 meaningful clusters were identified by the analysis. For heatmaps rlog counts from DESeq2
804 analysis were scaled by row (row Z-score) and low to high expression levels are indicated by
805 blue-white-red color gradient. 2 representative biological replicates are shown for each
806 sample in the figures for visualization purposes, count data from all replicates are available
807 in the Table S6.
808

809 ## Chromatin immunoprecipitation (ChIP)

810 For the ChIP with formaldehyde crosslinking, macrophages (3-10 x 10^6 cells per condition, 2-
811 4 biological replicates/ macrophage donors per condition, see Table S17) were washed once
812 with warm PBS and incubated for 30 min at 37 °C with accutase (eBioscience) to detach the
813 cells. ChIP protocol steps were performed as described in (Günther et al., 2016), except that
814 BSA-blocked ChIP grade protein A/G magnetic beads (Thermo Fisher Scientific) were added
815 to the chromatin and antibody mixture and incubated for 2 h at 4 °C rotating to bind
816 chromatin-antibody complexes. Samples were incubated for ~3 min with a magnetic stand
817 to ensure attachment of beads to the magnet and mixed by pipetting during the wash steps.
818 Eluted DNA was either subjected to ChIP-seq library preparation or used for ChIP-qPCR
819 experiments. Input chromatin DNA was prepared from 1/4 of chromatin amount used for
820 ChIP. Antibodies used for ChIP were anti-H3K4me3 (Merck Millipore, 04–745, 4 µl per ChIP),
821 anti-H3K27me3 (Merck Millipore, 07-449, 4 µl per ChIP), anti-H3K27ac (abcam, ab4729, 4 µg
822 per ChIP) and anti-H3K4me1 (Cell Signaling, 5326S, 5 µl per ChIP).
823
824

825 ## ChIP library preparation and sequencing

826 ChIP-seq libraries were constructed with 1-10 ng of ChIP DNA or input control as a starting
827 material. Libraries were generated using the NEXTflex™ ChIP-Seq Kit (Bioo Scientific) as per
828 manufacturer's recommendations. Concentrations of all samples were measured with a
829 Qubit Fluorometer (Thermo Fisher Scientific) and fragment length distribution of the final
830 libraries was analyzed with the DNA High Sensitivity Chip on an Agilent 2100 Bioanalyzer
831 (Agilent Technologies). All samples were normalized to 2 nM and pooled equimolar. The
832 library pool was sequenced on the NextSeq500 (Illumina) with 1 x 75 bp and total 18.6 to 41
833 million reads per sample.

834

835 ## ChIP-seq analysis

836 Sequencing reads containing bases with low quality scores (quality Phred score cutoff 20) or
837 adapters were trimmed using TrimGalore program
838 (http://www.bioinformatics.babraham.ac.uk/projects/trim_galore/). BWA (Li & Durbin, 2009)
839 was used to align reads from FASTQ files to hg19 human reference genome. Samtools (Liet
840 et al., 2009) was used for manipulations (e.g. sorting, indexing, conversions) of the
841 sequencing files. Picard (https://broadinstitute.github.io/picard/) was used for duplicate
842 read removal. BEDTools (Quinlan & Hall, 2010) was used for generation of BED files. The
843 following command was used for the alignment to hg19:
844 *bwa mem -M <reference genome> <ChIP-seqfile.fastq> | samtools view -bT <reference*
845 *genome> | samtools view -b -q 30 -F 4 -F 256 > <aligned-ChIP-seq-file.bam>*

846

847 ChIP-seq data have been deposited in the ArrayExpress database at EMBL-EBI
848 (www.ebi.ac.uk/arrayexpress) under accession number E-MTAB-10475.

849 ## ChIP-seq peak calling

850 MACS2 peak calling (Zhang et al., 2008) against the input control was used for H3K4me3 and
851 H3K27ac with *-q 0.01* parameter. SICER peak calling (Zang et al., 2009) against the input
852 control was used for H3K4me1 and H3K27me3 with default settings. SICER peaks for ChIP
853 enrichment over background with fold change ≥ 2 were selected. MACS2 and SICER peaks
854 were filtered to exclude blacklisted regions (Amemiya et al., 2019). To generate a file with all
855 peaks for each modification, peaks found in replicates for different conditions were pooled
856 together and merged using BEDTools (Quinlan & Hall, 2010).

857

858 ## ChIP-seq differential region analysis

859 DiffReps (Shen et al., 2013) was used for identification of differentially enriched regions/
860 dynamic regions between all collected biological replicates (see Table S17) from mock, WAC,
861 WA314, WA314ΔYopP and WA314ΔYopM. Csaw (Lun & Smyth, 2015) normalization
862 coefficients for efficiency bias were calculate with *width 150, spacing 100, minq 50, ext 210*
863 and used as input normalization coefficients in diffReps. Other diffReps parameters were set
864 to default except for H3K4me1 and H3K27me3 where *–nsd broad* parameter was used.
865 Accuracy of differentially enriched regions was examined in IGV (Thorvaldsdóttir et al., 2012).
866 Statistically significant sites with log2 FC ≥1 and adjusted P-value ≤0.05 were selected for
867 further analysis. Regions were further filtered to exclude regions that do not overlap MACS2
868 or SICER peaks, overlap blacklist regions (Amemiya et al., 2019) and regions with low read
869 counts (less than 20 for any replicate in the upregulated condition; less than 20 in the
870 upregulated condition for H3K4me3). Additionally, H3K27me3 regions with length less than
871 1700 bp were excluded as smaller regions appeared to be false positives. For further

872 clustering analysis of H3K4me3 and H3K27ac dynamic regions at promoters and enhancers
873 all differential sites for each mark for different conditions were pooled together and merged.
874

875 ## ChIP-seq quantification of tag counts

876 For quantification of tag counts at peaks and differential sites raw counts at target regions
877 were quantified using EaSeq (Lerdrup et al., 2016) and normalized with csaw (Lun & Smyth,
878 2015) efficiency bias coefficients with the formula: *(1+raw counts)/(csaw effective library*
879 *size/10^6)/bp per kb*.
880

881 ## ChIP-seq classification and annotation of regions

882 Promoter coordinates of ±2 kb from TSS and associated gene annotations were extracted
883 from RefSeq hg19 gene annotations in UCSC Genome Browser (Haeussler et al., 2018) using
884 EaSeq (Lerdrup et al., 2016). Regions overlapping promoter coordinates were defined as
885 regions at promoters and annotated with associated genes; one region could overlap
886 multiple promoters and associate with multiple genes. Regions that did not overlap
887 promoters but overlapped with H3K4me1 regions were assigned to enhancers. Enhancer
888 regions were annotated to the closest gene in EaSeq. The remaining regions were classified
889 as “undefined”.
890 For the identification of “dynamic” and “constant” peak regions, pooled peaks (based on
891 MACS2 or SICER) were intersected with pooled differential site regions (based on diffReps)
892 for each histone modification. Peaks intersecting differential regions were defined as
893 “dynamic”, whereas the rest of the peaks were termed “constant”.

894 Latent enhancers were defined as sites outside promoters with H3K4me1 signal increase
895 based on diffReps without pre-existing H3K4me1 and H3K27ac signal (no SICER and MACS2
896 peaks)
897

898 ChIP-seq clustering of promoters and enhancer regions

899 Clustering of normalized tag counts at pooled differential sites was performed
900 with R function heatmap.2. All H3K4me3 and H3K27ac regions from pooled differential sites
901 that intersected promoter regions were used for promoter (P1a-P2d classes) heatmaps. For
902 the H3K27ac enhancer heatmap (E1-E4 classes) all H3K27ac regions from pooled differential
903 sites outside promoters and overlapping H3K4me1 peaks were used. H3K4me3 promoter
904 heatmap was generated with clustering distance based on Pearson correlation and
905 Complete clustering method. For H3K27ac promoter heatmap regions which did not overlap
906 regions in H3K4me3 promoter heatmap were used for clustering. H3K27ac promoter and
907 enhancer heatmaps were generated with clustering distance based on Spearman correlation
908 and Average clustering method. Clustering distance, clustering method and number of
909 clusters were selected so that all meaningful clusters were identified by the analysis. Clusters
910 were further assembled into classes based on the pattern of histone modifications across
911 conditions.
912

913 ChIP-seq comparison to public data

914 For comparison of H3K27ac data from this study and publicly available data (Park et al., 2017;
915 Novakovic et al., 2016) raw tag counts at all H3K27ac peaks from this study were normalized
916 with csaw (Lun & Smyth, 2015) efficiency bias coefficients. Batch effect between different

917 datasets was removed using limma package (Ritchie et al., 2015) and tag counts used to
918 calculate Spearman correlation.
919

920 ## ChIP-qPCR

921 ChIP-qPCR was performed with SYBR Green/ROX qPCR Master Mix kit (Thermo Fisher
922 Scientific) following manufacturer's instructions. Primers (S15 Table) were designed using
923 PRIMER-Blast tool (Ye et al., 2012) with the optimal melting temperature of 60 °C and
924 template length between 55 and 200 bp. For all primer pairs input chromatin DNA was used
925 to generate standard curves and verify amplification efficiency between 90-100 %. The
926 specificity of primers was confirmed using reaction without a DNA template and melting
927 curve analysis of PCR products. qPCR was performed on a Rotorgene 6000 qPCR machine
928 (Qiagen) and analyzed with the Rotor-Gene 6000 software (Qiagen). A gain optimization was
929 carried out at the beginning of the run. Concentration of amplified DNA was calculated
930 based on the standard curve. In order to compare changes in enrichment at specific regions
931 between different conditions, normalization was done with at least 2 selected control
932 regions which did not show change in histone modifications during infection.
933

934 ## RT-qPCR analysis

935 Uninfected or infected primary human macrophages were subjected to RNA extraction using
936 RNeasy Mini Kit (Qiagen) following manufacturer's instructions. 1 µg of each RNA was
937 reverse transcribed using iScript cDNA Synthesis Kit (Bio-Rad Hercules) and subjected to RT-
938 qPCR reaction using the TaqMan Fast Advanced Master mix (Applied Biosystems) or SYBR
939 Green/ROX qPCR Master Mix kit (Thermo Fisher Scientific) and gene specific primers (see
940 Table S15 for primers).

941 For determination of IL1B and TNF mRNA levels the TaqMan Gene Expression Assays for
942 human IL1B (Hs00174097_m1) and TNF (Hs01113624_g1) were employed. As reference the
943 TagMan Gene Expression Assay for GAPDH (Hs02758991_g1), TATA-box binding protein (TBP)
944 (Hs00427620_m1) and beta-2-microglobulin (B2M) (Hs00187842_m1) was used (all from
945 Thermo Fisher Scientific). PCR was performed using the LightCycler 480 Instrument (Roche
946 Life Science) and data were analyzed according to manufacturer's instruction (Roche
947 LightCycler 480 software; Software release 1.5.1.62). Reference genes and external
948 standards were employed for the relative quantification of gene expression.
949 For determination of PPARGC1B and ABI1 mRNA levels RT-qPCR was performed with SYBR
950 Green/ROX qPCR Master Mix kit (Thermo Fisher Scientific) following manufacturer's
951 instructions. Primers (S15 Table) were designed using PRIMER-Blast tool (Ye et al., 2012)
952 with the optimal melting temperature of 60 °C, template length between 55 and 200 bp and
953 including intron junctions. cDNA was used to generate standard curves and verify
954 amplification efficiency between 90-100 %. The specificity of primers was confirmed using
955 reaction without a cDNA template or reverse transcription reaction without the reverse
956 transcriptase and melting curve analysis of PCR products. qPCR was performed on a
957 Rotorgene 6000 qPCR machine (Qiagen) and analyzed with the Rotor-Gene 6000 software
958 (Qiagen). A gain optimization was carried out at the beginning of the run. Concentration of
959 amplified cDNA was calculated based on the standard curve and normalized using reference
960 genes GAPDH and HPRT.
961
962
963
964

965 ## Pathway analysis

966 Gene Ontology (GO) and Kyoto Encyclopedia of Genes and Genomes (KEGG) terms were
967 determined for RNA-seq and ChIP-seq gene lists by using DAVID webtool (Huang et al., 2008;
968 Huang et al., 2009).

969

970 ## Motif analysis

971 Transcription factor (TF) motif enrichment for known motifs was performed using HOMER
972 package (Heinz et al., 2010). Command *findMotifsGenome.pl* was used and a list of genomic
973 coordinates was supplied as an input; the exact size of supplied regions was used by setting
974 parameter *-size given*.

975

976 ## Boxplots

977 Boxplots were generated using ggplot2 in R. Boxes encompass the twenty-fifth to
978 seventy-fifth percentile changes. Whiskers extend to the tenth and ninetieth percentiles.
979 Outliers are depicted with black dots. The central horizontal bar indicates the median.

980

981 ## Association between RNA-seq and ChIP-seq

982 Gene lists from RNA-seq and ChIP-seq were compared based on gene symbols to
983 find the number of overlapping genes and determine how many genes showed associated
984 epigenetic and gene expression changes. In some cases RNA-seq lists contained old gene
985 symbols which did not match to symbols in ChIP-seq lists with RefSeq annotation from UCSC.
986 All old symbols in RNA-seq lists without a match in RefSeq annotation were replaced with
987 the new symbol using Multi-symbol checker tool (Braschi et al., 2019).

988 Relative overlap between promoter and enhancer classes was obtained by dividing the
989 number of overlapping genes from two input classes with the total number of genes from
990 the first input class and then with total number of genes from the second input class.
991

992 ## Calculation of % YopP effect

993 Percentage YopP effect was calculated as ratio of FC between WA314ΔYopP vs
994 WA314 and WAC vs WA314 (Suppression and Prevention) or WA314 vs mock (Up
995 and Down). % YopP effect was presented for individual strongly WA314-regulated genes and
996 regions from inflammatory response and Rho GTPase pathway, which associated with gene
997 expression and histone modification changes in Suppression and Prevention profiles.
998 Specifically, only genes were selected, which overlapped WAC vs WA314 DEGs and
999 differentially enriched regions. Normalized tag counts were calculated for the target regions
1000 and used to obtain FC.
1001

1002 ## Rho GTPase pathway gene analysis

1003 The target gene list with 534 Rho GTPase pathway genes was compiled from publicly
1004 available data and included 370 effectors binding GTP-Rho GTPases (Bustelo et al., 2007;
1005 Bagci et al., 2020; Paul et al., 2017), 66 GAPs, 77 GEFs (Müller et al., 2020) and 23 Rho
1006 GTPases (Wennerberg & Der, 2004; Senoo et al., 2019 list in the supplementary). The list of
1007 genes does not match the list including activities (534 vs 536) as some genes possess
1008 multiple activities.
1009

1010

1011 ## Immunofluorescence staining

1012 For analysis of YopP effect on actin and ABI1 infected cells were washed twice with PBS,
1013 fixed with 4 % PFA in PBS for 5 min and permeabilized with 0.1 % Triton X-100 (w/v) in PBS
1014 for 10 min. After fixation and permeabilization coverslips were washed twice with PBS.
1015 Unspecific binding sites were blocked with 3 % bovine serum albumin (BSA, w/v) in PBS for
1016 at least 30 min. Samples were then incubated with 1:100 (anti-ABI1 (Sigma-Aldrich), anti-ZO-
1017 1 (Zymed), anti-H3K27ac (Abcam)) or 1:200 (anti-vinculin (Sigmal-Aldrich)) dilution of the
1018 primary antibody for 1 h and incubated with a 1:200 dilution of the suitable fluorophore-
1019 coupled secondary antibody for 45 min. Secondary anti-IgG antibodies and dyes used:
1020 Alexa488 chicken anti-rabbit (Molecular Probes), Alexa568 goat anti-mouse (Molecular
1021 Probes), AlexaFluor568 phalloidin (Invitrogen, GIBCO), AlexaFluor633 phalloidin (Invitrogen,
1022 GIBCO).
1023 After each staining coverslips were washed three times with PBS. Both primary and
1024 secondary antibodies were applied in PBS supplemented with 3 % BSA. Fluorophore-coupled
1025 phalloidin (1:200, Invitrogen) was added to the secondary antibody staining solution as
1026 indicated. Coverslips were mounted in ProLong Diamond (Thermo Fisher Scientific).
1027 For analysis of cells positive for effector translocation primary human macrophages were
1028 infected with different MOIs (10, 25, 50 and 100) of *Y. enterocolitica* WA314-YopE-ALFA
1029 strain for 6 h and fixed with 4 % PFA for 10 min. The samples were permeabilized with 0.1 %
1030 Triton-X-100 for 15 min, blocked with 3 % BSA for 1h and incubated with anti-ALFA
1031 nanobody-635 (FluoTag-X2 anti-ALFA Abberior Star 635P) (1:300) for 1h at RT. After washing
1032 3 times with PBS, the cells were counterstained with DAPI and phalloidin- 488 and mounted
1033 on glass slides in Prolong Glass Antifade Mountant (Thermo Fisher Scientific).
1034

1035 ## Microscopy

1036 Fixed samples were analyzed with a confocal laser scanning microscope (Leica TCS SP8)
1037 equipped with a 63x, NA1.4 oil immersion objective and Leica LAS X SP8 software (Leica
1038 Microsystems) was used for acquisition.

1039

1040 ## Image analysis

1041 For analysis of YopP effect on actin and ABI1 the z-stacks of images were combined to one
1042 image using maximum intensity projection. These images were used to measure the mean
1043 fluorescent intensity of the F-actin signal with a circle (9.02 µm diameter) around the cellular
1044 junctions between macrophages. The signal intensity at junctions refers to the maximum
1045 value of 255 for 8-bit images.

1046

1047 ## Western blot analysis

1048 Primary human macrophages (1-2*10^6 cells per condition) were washed once with warm PBS
1049 and scrapped off the plates to harvest the cells. Cell were pelleted by centrifugation at 700 x
1050 g, 10 min and 4°C. For ABI1 western blot cells were resuspended in 60 µl Lysis buffer (50 mM
1051 HEPES-KOH, pH 7.5, 140 mM NaCl, 1 mM EDTA, 10 % glycerol, 0.5 % NP-40, 0.75 % Triton X-
1052 100, protease inhibitor (Complete, Roche Diagnostics) and lyzed by incubation at 4°C for 30
1053 min. For caspase-3 western blot cells were resuspended in 40 µl RIPA buffer (50 mM Tris, pH
1054 8.0, 150 mM NaCl, 1 % TRITON-X-100, 0.5 % sodium deoxycholate, 0.1 % SDS, protease
1055 inhibitor (Complete, Roche Diagnostics) and lyzed by incubation at 4°C for 10 min and brief
1056 sonication. Lysates were centrifuged at 10000 x g, 10 min and 4°C and supernantant was
1057 collected for Western blot analysis.

1058 Proteins were separated by SDS-PAGE and transferred to polyvinylidene difluoride (PVDF)
1059 membrane (Immobilion-P, Millipore) by semi-dry blotting. The membrane was incubated in
1060 blocking solution (5 % milk powder (w/v) for ABI1 or 3 % BSA (w/v) for GAPDH and caspase-3
1061 in TBS supplemented with 0.03 % Tween 20; TBS-T) at room temperature for 30 min. Primary
1062 antibody incubations (anti-ABI1 (Sigma-Aldrich) at 1:1000, anti-GAPDH (Sigma-Aldrich) at
1063 1:3000, anti-caspase-3 (Cell Signaling) at 1:1000) were carried out at 4°C overnight,
1064 secondary antibody incubation (horseradish peroxidase linked anti-rabbit IgG (Cell Signaling)
1065 at 1:10000) was performed at room temperature for 1 h. Washing steps with TBS-T were
1066 done between the incubations. Antibody signals were visualized with chemiluminescence
1067 technology (Supersignal West Femto, Pierce Chemical) and captured on X-ray films (Fujifilm)
1068 or digital imager (Licor).
1069

1070 ## Ethics statement

1071 Approval for the analysis of anonymized blood donations (WF-015/12) was obtained by the
1072 Ethical Committee of the Ärztekammer Hamburg (Germany).
1073
1074

1075 # Acknowledgements

1076 We thank the UKE Core Facility Microscopy Imaging (Umif) for help with experimental setups
1077 and data analysis. We also would like to thank Daniela Indenbirken for generating the RNA-
1078 seq libraries and Frank Bentzien (UKE Transfusion Medicine) for buffy coats. We thank
1079 Alexander Carsten and Asiri Ortega for WA314-YopE-ALFA strain and Eva Tolosa and
1080 Manuela Kolster for flow cytometry analysis.

1081

1082

1083 # References

1084 Aepfelbacher, M. & Wolters, M. in The Actin Cytoskeleton and Bacterial Infection 201–220
1085 (Springer International Publishing, Cham, 2017).

1086 Aktories, K., Schmidt, G. & Just, I. Rho GTPases as Targets of Bacterial Protein Toxins. Biological
1087 Chemistry **381,** 421 –426 (2000).

1088 Aktories, K. Bacterial protein toxins that modify host regulatory GTPases. Nature reviews.
1089 Microbiology **9,** 487—498 (2011).

1090 Allis, C. D. & Jenuwein, T. The molecular hallmarks of epigenetic control. Nature Reviews
1091 Genetics **17,** 487–500 (2016).

1092 Amemiya, H. M., Kundaje, A. & Boyle, A. P. The ENCODE Blacklist: Identification of Problematic
1093 Regions of the Genome. Scientific Reports **9,** 9354 (2019).

1094 Aspenström, P., Ruusala, A. & Pacholsky, D. Taking Rho GTPases to the next level: The cellular
1095 functions of atypical Rho GTPases. Experimental Cell Research **313,** 3673 –3679 (2007).

1096 Auerbuch, V., Golenbock, D. T. & Isberg, R. R. Innate Immune Recognition of Yersinia
1097 pseudotuberculosis Type III Secretion. PLOS Pathogens **5**, 1–16 (2009).

1098 Bagci, H. et al. Mapping the proximity interaction network of the Rho-family GTPases reveals
1099 signalling pathways and regulatory mechanisms. Nature cell biology **22,** 120—134 (2020).

1100 Balada-Llasat, J.-M. & Mecsas, J. Yersinia Has a Tropism for B and T Cell Zones of Lymph
1101 Nodes That Is Independent of the Type III Secretion System. PLOS Pathogens **2,** 1–13 (2006).

1102 Barski, A. et al. High-Resolution Profiling of Histone Methylations in the Human Genome. Cell
1103 **129,** 823—837 (2007).

1104 Bedi, R., Du, J., Sharma, A. K., Gomes, I. & Ackerman, S. J. Human C/EBP-E activator and
1105 repressor isoforms differentially reprogram myeloid lineage commitment and differentiation.
1106 Blood **113,** 317–327 (2009).

1107 Berneking, L. et al. Immunosuppressive Yersinia Effector YopM Binds DEAD Box Helicase
1108 DDX3 to Control Ribosomal S6 Kinase in the Nucleus of Host Cells. PLoS Pathogens **12,** 1–35 (2016).

1109 Bierne, H., Hamon, M. & Cossart, P. Epigenetics and Bacterial Infections. Cold Spring Harbor
1110 Perspectives in Medicine **2** (2012).
1111 Bohn, E. et al. Gene expression patterns of epithelial cells modulated by pathogenicity factors
1112 of Yersinia enterocolitica†. Cellular Microbiology **6**, 129–141 (2004).
1113 Bokoch, G. M. Regulation of innate immunity by Rho GTPases. Trends in Cell Biology **15,**
1114 163–171 (2005).
1115 Boureux, A., Vignal, E., Faure, S. & Fort, P. Evolution of the Rho Family of Ras-Like GTPases
1116 in Eukaryotes. Molecular Biology and Evolution **24,** 203–216 (2006).
1117 Braschi, B. et al. Genenames.org: the HGNC and VGNC resources in 2019. Nucleic Acids
1118 Research **47,** D786–D792 (2018).
1119 Brodsky, I. E. et al. A Yersinia Effector Protein Promotes Virulence by Preventing Inflammasome
1120 Recognition of the Type III Secretion System. Cell Host and Microbe **7,** 376 –387 (2010).
1121 Broz, P. & Dixit, V. M. Inflammasomes: mechanism of assembly, regulation and signalling.
1122 Nature reviews. Immunology **16,** 407—420 (2016).
1123 Bustelo, X. R., Sauzeau, V. & Berenjeno, I. M. GTP-binding proteins of the Rho/Rac family:
1124 regulation, effectors and functions in vivo. BioEssays **29,** 356–370 (2007).
1125 Carsten, A. et al. Visualization of bacterial type 3 secretion system components down to the
1126 molecular level by MINFLUX nanoscopy. bioRxiv (2021).
1127 Chakraborty, N. et al. The responses of lungs and adjacent lymph nodes in responding to
1128 Yersinia pestis infection: A transcriptomic study using a non-human primate model. PLOS ONE
1129 **14,** 1–24 (2019).
1130 Chardin, P. Function and regulation of Rnd proteins. Nature reviews. Molecular cell biology **7,**
1131 54—62 (2006).
1132 Chen, B. et al. Epigenetic activation of the small GTPase TCL contributes to colorectal cancer
1133 cell migration and invasion. Oncogenesis **9,** 86 (2020).
1134 Chen, X. et al. Ena/VASP Proteins Cooperate with the WAVE Complex to Regulate the Actin
1135 Cytoskeleton. Developmental Cell **30,** 569–584 (2014).

1136 Christgen, S., Place, D. E. & Kanneganti, T.-D. Toward targeting inflammasomes: insights into
1137 their regulation and activation. Cell research **30,** 315—327 (2020).
1138 Chung, L. K. et al. The Yersinia Virulence Factor YopM Hijacks Host Kinases to Inhibit Type III
1139 Effector-Triggered Activation of the Pyrin Inflammasome. Cell Host and Microbe **20,** 296 –306
1140 (2016).
1141 Comer, J. E. et al. Transcriptomic and Innate Immune Responses to Yersinia pestis in
1142 the Lymph Node during Bubonic Plague. Infection and Immunity **78,** 5086–5098 (2010)
1143 Connor, M. G. et al. Yersinia pestis Targets the Host Endosome Recycling Pathway during the
1144 Biogenesis of the Yersinia-Containing Vacuole To Avoid Killing by Macrophages.
1145 mBio **9,** e01800–17 (2018).
1146 Connor, M., Arbibe, L. & Hamon, M. Customizing Host Chromatin: a Bacterial Tale. Microbiology
1147 Spectrum **7** (2019).
1148 Cornelis, G. R. & Wolf-Watz, H. The Yersinia Yop virulon: a bacterial system for subverting
1149 eukaryotic cells. Molecular Microbiology **23,** 861–867 (1997).
1150 Diacovich, L. & Gorvel, J.-P. Bacterial manipulation of innate immunity to promote infection.
1151 Nature Reviews Microbiology **8,** 117–128 (2010).
1152 Dobin, A. et al. STAR: ultrafast universal RNA-seq aligner. Bioinformatics **29,** 15–21 (2012).
1153 Dong, W. & Hamon, M. A. Revealing eukaryotic histone-modifying mechanisms through bacterial
1154 infection. Seminars in Immunopathology **42,** 201–213 (2020).
1155 Doyle, S. E. et al. Toll-like Receptors Induce a Phagocytic Gene Program through p38. Journal
1156 of Experimental Medicine **199,** 81–90 (2004).
1157 Drechsler-Hake, D. et al. Mononuclear phagocytes contribute to intestinal invasion and dissemination
1158 of Yersinia enterocolitica. International Journal of Medical Microbiology **306,** 357–366 (2016).
1159 Fritz, G., Just, I. & Kaina, B. Rho GTPases are over-expressed in human tumors. International
1160 Journal of Cancer **81,** 682–687 (1999).
1161 Gallant, S. & Gilkeson, G. ETS transcription factors and regulation of immunity. Archivum
1162 Immunologiae et Therapiae Experimentalis **54,** 149–163 (2006).

1163 Galán, J. E. & Wolf-Watz, H. Protein delivery into eukaryotic cells by type III secretion machines.
1164 Nature **444,** 567—573 (2006).
1165 Gao, P. et al. Transcription factor Fli-1 positively regulates lipopolysaccharide-induced interleukin-27
1166 production in macrophages. Molecular immunology **71,** 184—191 (2016).
1167 Glass, C. K. & Natoli, G. Molecular control of activation and priming in macrophages. Nature
1168 immunology **17,** 26–33 (2015).
1169 Grassl, G. A. et al. Activation of NF-κB and IL-8 by Yersinia enterocolitica invasin protein is
1170 conferred by engagement of Rac1 and MAP kinase cascades. Cellular Microbiology **5,** 957–
1171 971 (2003).
1172 Grootjans, S. et al. A real-time fluorometric method for the simultaneous detection of cell death
1173 type and rate. Nature Protocols **11,** 1444–1454 (2016).
1174 Günther, T., Theiss, J. M., Fischer, N. & Grundhoff, A. Investigation of Viral and Host Chromatin by
1175 ChIP-PCR or ChIP-Seq Analysis. Current Protocols in Microbiology **40,** 1E.10.1–1E.10.21 (2016).
1176 Göös, H. et al. Gain-of-function CEBPE mutation causes noncanonical autoinflammatory
1177 inflammasomopathy. Journal of Allergy and Clinical Immunology **144,** 1364–1376 (2019).
1178 Haeussler, M. et al. The UCSC Genome Browser database: 2019 update. Nucleic Acids Research **47,**
1179 D853–D858 (2018).
1180 Haga, R. B. & Ridley, A. J. Rho GTPases: Regulation and roles in cancer cell biology. Small
1181 GTPases **7,** 207–221 (2016).
1182 Hammamieh, R. et al. Temporal Progression of Pneumonic Plague in Blood of Nonhuman Primate: A
1183 Transcriptomic Analysis. PLOS ONE **11,** 1–21 (Mar. 2016).
1184 Heasman, S. J. & Ridley, A. J. Mammalian Rho GTPases: new insights into their functions
1185 from in vivo studies. Nature reviews. Molecular cell biology **9,** 690—701 (2008).
1186 Heesemann, J & Laufs, R. Construction of a mobilizable Yersinia enterocolitica virulence plasmid.
1187 Journal of Bacteriology **155,** 761–767 (1983).
1188 Heine, W. et al. Loss of CNFY toxin-induced inflammation drives Yersinia pseudotuberculosis
1189 into persistency. PLOS Pathogens **14,** 1–32 (2018).

1190 Heintzman, N. D. et al. Histone modifications at human enhancers reflect global cell type-specific
1191 gene expression. Nature **459,** 108–112 (2009).
1192 Heinz, S. et al. Simple Combinations of Lineage-Determining Transcription Factors Prime cis-
1193 Regulatory Elements Required for Macrophage and B Cell Identities. Molecular Cell **38,** 576–589
1194 (2010).
1195 Hodge, R. G. & Ridley, A. J. Regulating Rho GTPases and their regulators. Nature reviews.
1196 Molecular cell biology **17,** 496—510 (2016).
1197 Hoffmann, R., Van Erp, K., Trülzsch, K. & Heesemann, J. Transcriptional responses of murine
1198 macrophages to infection with Yersinia enterocolitica. Cellular Microbiology **6,** 377–390 (2004).
1199 Hop, H. T. et al. The Key Role of c-Fos for Immune Regulation and Bacterial Dissemination in
1200 Brucella Infected Macrophage. Frontiers in Cellular and Infection Microbiology **8,** 287 (2018).
1201 Huang, D. W., Sherman, B. T. & Lempicki, R. A. Bioinformatics enrichment tools: paths toward
1202 the comprehensive functional analysis of large gene lists. Nucleic Acids Research **37,** 1–13 (2008).
1203 Huang, D. W., Sherman, B. T. & Lempicki, R. A. Systematic and integrative analysis of large
1204 gene lists using DAVID bioinformatics resources. Nature Protocols **4,** 44–57 (2009).
1205 Ivashkiv, L. B. Epigenetic regulation of macrophage polarization and function. Trends in Immunology
1206 **34,** 216 –223 (2013).
1207 Jaffe, A. B. & Hall, A. RHO GTPASES: Biochemistry and Biology. Annual Review of Cell and
1208 Developmental Biology **21,** 247–269 (2005).
1209 Kang, K. et al. IFN- selectively suppresses a subset of TLR4-activated genes and enhancers
1210 to potentiate macrophage activation. Nature Communications **10** (2019).
1211 Köberle, M. et al. Yersinia enterocolitica YopT and Clostridium difficile Toxin B Induce Expression of
1212 GILZ in Epithelial Cells. PLOS ONE **7,** 1–17 (2012).
1213 Klemm, S. L., Shipony, Z. & Greenleaf,W. J. Chromatin accessibility and the regulatory epigenome.
1214 Nature reviews. Genetics **20,** 207—220 (2019).
1215 Koch, I., Dach, K., Heesemann, J. & Hoffmann, R. Yersinia enterocolitica inactivates NK cells.
1216 International Journal of Medical Microbiology **303,** 433–442 (2013).

1217 Kopp, P. et al. The Kinesin KIF1C and Microtubule Plus Ends Regulate Podosome Dynamics
1218 in Macrophages. Molecular Biology of the Cell **17,** 2811–2823 (2006).
1219 Laurin, M. & Côté, J.-F. Insights into the biological functions of Dock family guanine nucleotide
1220 exchange factors. Genes and Development **28,** 533–547 (2014).
1221 Lennard Richard, M. L. et al. The Fli-1 transcription factor regulates the expression of CCL5/RANTES.
1222 Journal of immunology (Baltimore, Md. : 1950) **193,** 2661—2668 (2014).
1223 Lerdrup, M., Johansen, J. V., Agrawal-Singh, S. & Hansen, K. An interactive environment for
1224 agile analysis and visualization of ChIP-sequencing data. Nature Structural & Molecular Biology
1225 **23,** 349–357 (2016).
1226 Li, H. & Durbin, R. Fast and accurate short read alignment with Burrows–Wheeler transform.
1227 Bioinformatics **25,** 1754–1760 (2009).
1228 Li, H. et al. The Sequence Alignment/Map format and SAMtools. Bioinformatics **25,** 2078–
1229 2079 (2009).
1230 Liao, Y., Smyth, G. K. & Shi, W. featureCounts: an efficient general purpose program for assigning
1231 sequence reads to genomic features. Bioinformatics (Oxford, England) **30,** 923—930
1232 (2014).
1233 Lopes Fischer, N., Naseer, N., Shin, S. & Brodsky, I. E. Effector-triggered immunity and pathogen
1234 sensing in metazoans. Nature Microbiology **5,** 14–26 (2020).
1235 Love, M. I., Huber, W. & Anders, S. Moderated estimation of fold change and dispersion for
1236 RNA-seq data with DESeq2. Genome Biology **15,** 550 (2014).
1237 Lun, A. T. & Smyth, G. K. csaw: a Bioconductor package for differential binding analysis of
1238 ChIP-seq data using sliding windows. Nucleic Acids Research **44,** e45–e45 (2015).
1239 Lupfer, C., Malik, A. & Kanneganti, T.-D. Inflammasome control of viral infection. Current Opinion in
1240 Virology **12.** Antiviral strategies • Virus structure and expression, 38 –46 (2015).
1241 Malsin, E. S., Kim, S., Lam, A. P. & Gottardi, C. J. Macrophages as a Source and Recipient of
1242 Wnt Signals. Frontiers in Immunology **10,** 1813 (2019).
1243 Marketon, M. M., DePaolo, R. W., DeBord, K. L., Jabri, B. & Schneewind, O. Plague Bacteria

1244 Target Immune Cells During Infection. Science **309,** 1739–1741 (2005).

1245 McPhee, J. B., Mena, P., Zhang, Y. & Bliska, J. B. Interleukin-10 Induction Is an Important
1246 Virulence Function of the Yersinia pseudotuberculosis Type III Effector YopM. Infection and
1247 Immunity **80** (ed Bäumler, A. J.) 2519–2527 (2012).

1248 Mogensen, T. H. Pathogen Recognition and Inflammatory Signaling in Innate Immune Defenses.
1249 Clinical Microbiology Reviews **22,** 240–273 (2009).

1250 Mott, H. R. & Owen, D. Structures of Ras superfamily effector complexes: What have we learnt in two
1251 decades? Critical Reviews in Biochemistry and Molecular Biology **50,** 85–133 (2015).

1252 Mukherjee, S. et al. Yersinia YopJ Acetylates and Inhibits Kinase Activation by Blocking
1253 Phosphorylation. Science **312,** 1211–1214 (2006).

1254 Müller, P. M. et al. Systems analysis of RhoGEF and RhoGAP regulatory proteins reveals spatially
1255 organized RAC1 signalling from integrin adhesions. Nature Cell Biology **22,** 498–511 (2020).

1256 Novakovic, B. et al. β-Glucan Reverses the Epigenetic State of LPS-Induced Immunological
1257 Tolerance. Cell **167,** 1354–1368.e14 (2016).

1258 Nuss, A. M. et al. Tissue dual RNA-seq allows fast discovery of infection-specific functions and
1259 riboregulators shaping host–pathogen transcriptomes. Proceedings of the National Academy of
1260 Sciences **114,** E791–E800 (2017).

1261 O'Reilly, D., Quinn, C. M., El-Shanawany, T., Gordon, S. & Greaves, D. R. Multiple Ets Factors
1262 and Interferon Regulatory Factor-4 Modulate CD68 Expression in a Cell Type-specific Manner.
1263 Journal of Biological Chemistry **278,** 21909–21919 (2003).

1264 Ostuni, R. et al. Latent Enhancers Activated by Stimulation in Differentiated Cells. Cell **152,**
1265 157–171 (2013).

1266 Pacis, A. et al. Gene activation precedes DNA demethylation in response to infection in human
1267 dendritic cells. Proceedings of the National Academy of Sciences **116,** 6938–6943 (2019).

1268 Park, S. H. et al. Type I IFNs and TNF cooperatively reprogram the macrophage epigenome
1269 to promote inflammatory activation. Nature immunology **18,** 1104 –1116 (2017).

1270 Paul, F. et al. Quantitative GTPase Affinity Purification Identifies Rho Family Protein Interaction
1271 Partners. Molecular & Cellular Proteomics **16,** 73–85 (2017).
1272 Phanstiel, D. H. et al. Static and Dynamic DNA Loops form AP-1-Bound Activation Hubs during
1273 Macrophage Development. Molecular Cell **67,** 1037–1048.e6 (2017).
1274 Philip, N. H., Zwack, E. E. & Brodsky, I. E. in Inflammasome Signaling and Bacterial Infections. 69–90
1275 (Springer International Publishing, Cham, 2016).
1276 Pujol, C. & Bliska, J. B. The Ability To Replicate in Macrophages Is Conserved between Yersinia
1277 pestis and Yersinia pseudotuberculosis. Infection and Immunity **71,** 5892–5899 (2003).
1278 Pujol, C. et al. Yersinia pestis Can Reside in Autophagosomes and Avoid Xenophagy
1279 in Murine Macrophages by Preventing Vacuole Acidification. Infection and Immunity **77,** 2251–
1280 2261 (2009).
1281 Quinlan, A. R. & Hall, I. M. BEDTools: a flexible suite of utilities for comparing genomic features.
1282 Bioinformatics **26,** 841–842 (2010).
1283 Rada-Iglesias, A. et al. A unique chromatin signature uncovers early developmental enhancers in
1284 humans. Nature **470,** 279–283 (2011).
1285 Reinés, M. et al. Deciphering the Acylation Pattern of Yersinia enterocolitica Lipid A. PLOS
1286 Pathogens **8,** 1–21 (2012).
1287 Ritchie, M. E. et al. limma powers differential expression analyses for RNA-sequencing and
1288 microarray studies. Nucleic Acids Research **43,** e47–e47 (2015).
1289 Roach, J. C. et al. Transcription factor expression in lipopolysaccharide-activated peripheral-blood-
1290 derived mononuclear cells. Proceedings of the National Academy of Sciences **104,** 16245–16250
1291 (2007).
1292 Rolando, M. et al. Legionella pneumophila Effector RomA Uniquely Modifies Host Chromatin
1293 to Repress Gene Expression and Promote Intracellular Bacterial Replication. Cell Host & Microbe
1294 **13,** 395 –405 (2013).
1295 Ruckdeschel, K et al. Interaction of Yersinia enterocolitica with macrophages leads to macrophage
1296 cell death through apoptosis. Infection and Immunity **65,** 4813–4821 (1997).

1297 Ruckdeschel, K. et al. Yersinia Outer Protein P of Yersinia enterocolitica Simultaneously Blocks
1298 the Nuclear Factor-κB Pathway and Exploits Lipopolysaccharide Signaling to Trigger Apoptosis
1299 in Macrophages. The Journal of Immunology **166,** 1823–1831 (2001).
1300 Ryan, D. G. & O'Neill, L. A. Krebs Cycle Reborn in Macrophage Immunometabolism. Annual
1301 Review of Immunology **38,** 289–313 (2020).
1302 Ryu, J. R., Echarri, A., Li, R. & Pendergast, A. M. Regulation of Cell-Cell Adhesion by Abi/Diaphanous
1303 Complexes. Molecular and Cellular Biology **29,** 1735–1748 (2009).
1304 Saeed, S. et al. Epigenetic programming of monocyte-to-macrophage differentiation and trained
1305 innate immunity. Science **345** (2014).
1306 Sarhan, J. et al. Caspase-8 induces cleavage of gasdermin D to elicit pyroptosis during Yersinia
1307 infection. Proceedings of the National Academy of Sciences **115,** E10888–E10897 (2018).
1308 Sauvonnet, N., Pradet-Balade, B., Garcia-Sanz, J. A. & Cornelis, G. R. Regulation of mRNA
1309 Expression in Macrophages afterYersinia enterocolitica Infection: ROLE OF DIFFERENT Yop
1310 EFFECTORS. Journal of Biological Chemistry **277,** 25133–25142 (2002).
1311 Sauvonnet, N., Lambermont, I., Bruggen, P. v. d. & Cornelis, G. R. YopH prevents monocyte
1312 chemoattractant protein 1 expression in macrophages and T-cell proliferation through inactivation of
1313 the phosphatidylinositol 3-kinase pathway. Molecular Microbiology **45,** 805–815 (2002)b
1314 Sawicka, A. & Seiser, C. Sensing core histone phosphorylation — A matter of perfect timing.
1315 Biochimica et Biophysica Acta (BBA) - Gene Regulatory Mechanisms **1839.** Molecular
1316 mechanisms of histone modification function, 711 –718 (2014).
1317 Schmid, Y. et al. Yersinia enterocolitica Adhesin A Induces Production of Interleukin-8 in
1318 Epithelial Cells. Infection and Immunity **72,** 6780–6789 (2004).
1319 Schubert, K. A., Xu, Y., Shao, F. & Auerbuch, V. The Yersinia Type III Secretion System as a
1320 Tool for Studying Cytosolic Innate Immune Surveillance. Annual Review of Microbiology **74,**
1321 221–245 (2020).
1322 Schulte, R. et al. Yersinia enterocolitica invasin protein triggers IL-8 production in epithelial cells
1323 via activation of Rel p65-p65 homodimers. The FASEB Journal **14,** 1471–1484 (2000).

1324 Senoo, H. et al. Phosphorylated Rho-GDP directly activates mTORC2 kinase towards AKT
1325 through dimerization with Ras-GTP to regulate cell migration. Nature cell biology **21,** 867—878
1326 (2019).
1327 Shen, L. et al. diffReps: Detecting Differential Chromatin Modification Sites from ChIP-seq
1328 Data with Biological Replicates. PLOS ONE **8,** 1–13 (2013).
1329 Spinner, J. L. et al. Yersinia pestis survival and replication within human neutrophil phagosomes
1330 and uptake of infected neutrophils by macrophages. Journal of Leukocyte Biology **95,** 389–398
1331 (2014).
1332 Stahnke, S. et al. Loss of Hem1 disrupts macrophage function and impacts migration, phagocytosis,
1333 and integrin-mediated adhesion. Current Biology **31,** 2051–2064.e8 (2021).
1334 Stiegler, A. L. & Boggon, T. J. The pseudoGTPase group of pseudoenzymes. The FEBS Journal
1335 **287,** 4232–4245 (2020).
1336 St. John, A. L. et al. S1P-Dependent Trafficking of Intracellular Yersinia pestis
1337 through Lymph Nodes Establishes Buboes and Systemic Infection. Immunity **41,** 440–450
1338 (2014).
1339 Subrahmanyam, Y. V. B. K. et al. RNA expression patterns change dramatically in human neutrophils
1340 exposed to bacteria. Blood **97,** 2457–2468 (2001).
1341 Tajadura-Ortega, V. et al. An RNAi screen of Rho signalling networks identifies RhoH as a
1342 regulator of Rac1 in prostate cancer cell migration. BMC Biology **16** (2018).
1343 Takeuchi, O. & Akira, S. Pattern Recognition Receptors and Inflammation. Cell **140,** 805 –820
1344 (2010).
1345 Tcherkezian, J. & Lamarche-Vane, N. Current knowledge of the large RhoGAP family of proteins.
1346 Biology of the Cell **99,** 67–86 (2007).
1347 Thorvaldsdóttir, H., Robinson, J. T. & Mesirov, J. P. Integrative Genomics Viewer (IGV):
1348 highperformance genomics data visualization and exploration. Briefings in Bioinformatics **14,** 178–
1349 192 (2012).

1350 Trülzsch, K., Sporleder, T., Igwe, E. I., Rüssmann, H. & Heesemann, J. Contribution of the Major
1351 Secreted Yops of Yersinia enterocolitica O:8 to Pathogenicity in the Mouse Infection
1352 Model. Infection and Immunity **72,** 5227–5234 (2004).
1353 Verger, A. & Duterque-Coquillaud, M. When Ets transcription factors meet their partners.
1354 BioEssays **24,** 362–370 (2002).
1355 Viboud, G. I. & Bliska, J. B. YERSINIA OUTER PROTEINS: Role in Modulation of Host Cell
1356 Signaling Responses and Pathogenesis. Annual Review of Microbiology **59,** 69–89 (2005).
1357 Vincent, S, Jeanteur, P & Fort, P. Growth-regulated expression of rhoG, a new member of the ras
1358 homolog gene family. Molecular and Cellular Biology **12,** 3138–3148 (1992).
1359 Wang, Z. et al. Combinatorial patterns of histone acetylations and methylations in the human
1360 genome. Nature Genetics **40,** 897–903 (2008).
1361 Wennerberg, K. & Der, C. J. Rho-family GTPases: it's not only Rac and Rho (and I like it).
1362 Journal of Cell Science **117,** 1301–1312 (2004).
1363 Yamazaki, D., Oikawa, T. & Takenawa, T. Rac-WAVE-mediated actin reorganization is required for
1364 organization and maintenance of cell-cell adhesion. Journal of Cell Science **120,** 86–100 (2007).
1365 Ye, J. et al. Primer-BLAST: A tool to design target-specific primers for polymerase chain reaction. BMC
1366 Bioinformatics **13,** 134 (2012).
1367 Yun, M., Workman, J. L. & Li, B. Readers of histone modifications. Cell research **21,** 564–578
1368 (2011).
1369 Zang, C. et al. A clustering approach for identification of enriched domains from histone modification
1370 ChIP-Seq data. Bioinformatics **25,** 1952–1958 (2009).
1371 Zhang, Y., Ting, A. T., Marcu, K. B. & Bliska, J. B. Inhibition of MAPK and NF-κB Pathways Is
1372 Necessary for Rapid Apoptosis in Macrophages Infected with Yersinia. The Journal of Immunology
1373 **174,** 7939–7949 (2005).
1374 Zhang, X & Mosser, D. Macrophage activation by endogenous danger signals. The Journal of
1375 Pathology **214,** 161–178 (2008).
1376 Zhang, Y. et al. Model-based Analysis of ChIP-Seq (MACS). Genome Biology **9,** R137 (2008).

1377 Zhou, P. et al. Alpha-kinase 1 is a cytosolic innate immune receptor for bacterial ADP-heptose.
1378 Nature **561,** 122–126 (2018).
1379 Zipfel, P. A. et al. Role for the Abi/Wave Protein Complex in T Cell Receptor-Mediated Proliferation
1380 and Cytoskeletal Remodeling. Current Biology **16,** 35–46 (2006).
1381
1382

Figures

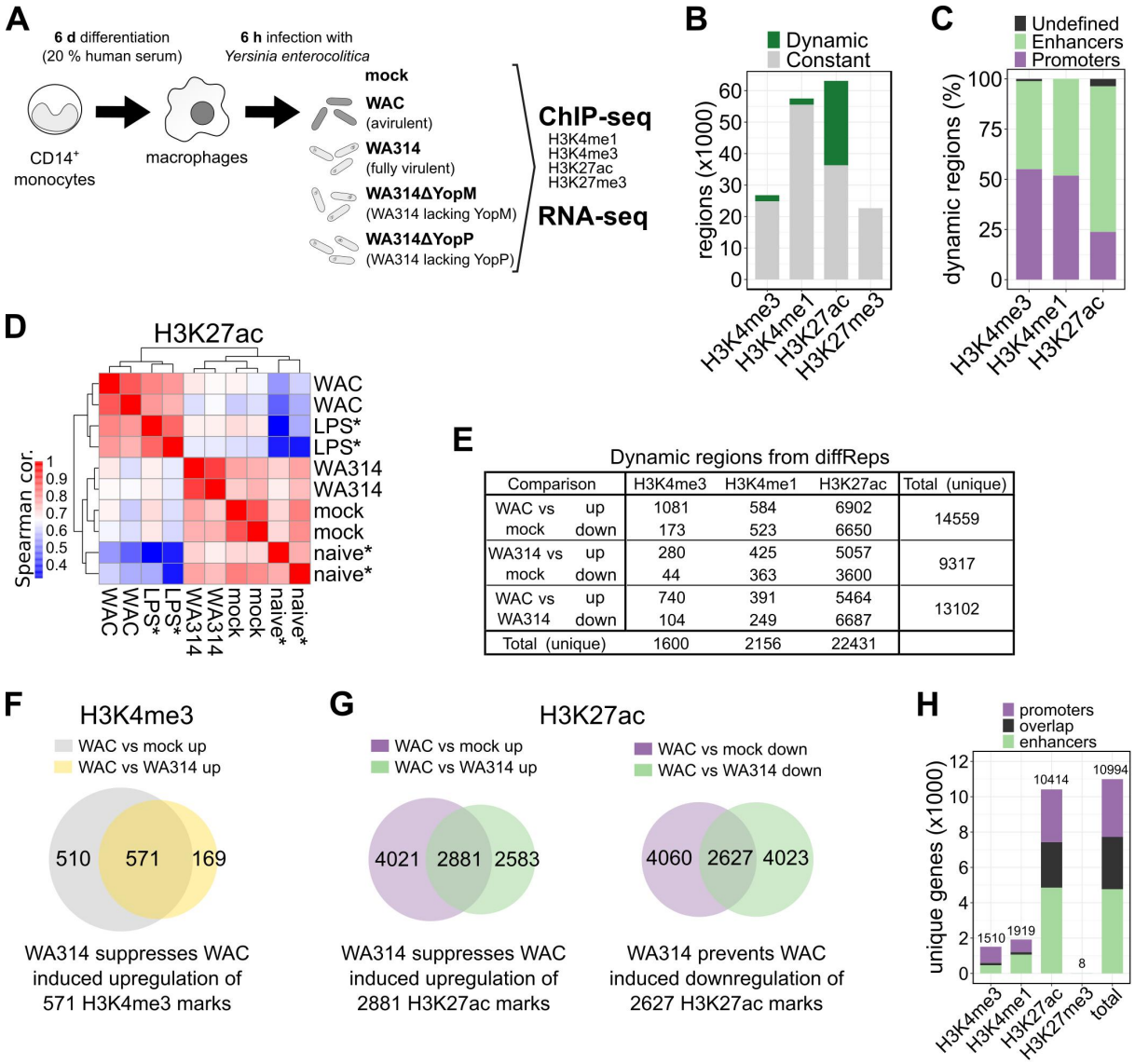

Fig 1. Changes of epigenetic histone modifications in *Y. enterocolitica* infected primary human macrophages.

A, Experimental design. CD14⁺ monocytes were isolated and differentiated into macrophages by cultivation with 20 % human serum for 6 days. Macrophages from ≥ two independent donors were mock infected or infected with avirulent *Y. enterocolitica* strain WAC, wild type strain WA314 or the single Yop-mutant strains WA314ΔYopM and WA314ΔYopP with multiplicity-of-infection (MOI) of 100 for 6 h. Samples were subjected to ChIP-seq for histone modifications H3K27ac, H3K4me3 and RNA-seq. H3K4me1 and

1393 H3K27me3 ChIP-seq was performed only for mock, WAC and WA314 infected macrophages.
1394 For all replicates used in the analysis see Table S17.
1395 **B,** Bar plot showing proportions of dynamic and constant regions of ChIP-seq data obtained
1396 from mock-, WAC- and WA314 infected macrophages as described in **(A)**. Dynamic regions
1397 were defined as MACS (H3K4me3, H3K27ac) or SICER (H3K4me1, H3K27me3) peaks
1398 overlapping significantly (≥ 2-fold change, adjusted P-value ≤ 0.05) up- or down-regulated
1399 differentially enriched regions from diffReps in the three pairwise comparisons WAC vs mock,
1400 WA314 vs mock and WAC vs WA314.
1401 **C,** Bar plot showing distribution of dynamic regions from **(B)** at gene promoters and
1402 enhancers.
1403 **D,** Heatmap showing Spearman correlation (cor.) of H3K27ac tag density at all H3K27ac
1404 peaks from mock-, WAC- and WA314-infected samples and publicly available H3K27ac ChIP-
1405 seq data of naive* and LPS* treated macrophages. Low to high correlation is indicated by
1406 blue-white-red colour scale.
1407 **E,** Number of differentially enriched regions (diffReps ≥ 2-fold change, adjusted P-value ≤
1408 0.05) for the indicated histone marks. Total (unique) refers to all unique regions in each row
1409 or column after merging overlapping regions.
1410 **F, G,** Venn diagrams showing overlaps of differentially enriched regions from diffReps
1411 depicting suppression of WAC induced upregulation of H3K4me3 marks by WA314 **(F)** and
1412 suppression of WAC induced up-regulation of H3K27ac marks by WA314 or prevention of
1413 WAC induced down-regulation of H3K27ac marks by WA314 **(G)**.
1414 **H,** Bar plot showing the number of genes associated with promoters, enhancers or both for
1415 the indicated histone marks associated with dynamic regions in **(E)** or when taking all regions
1416 together (total).

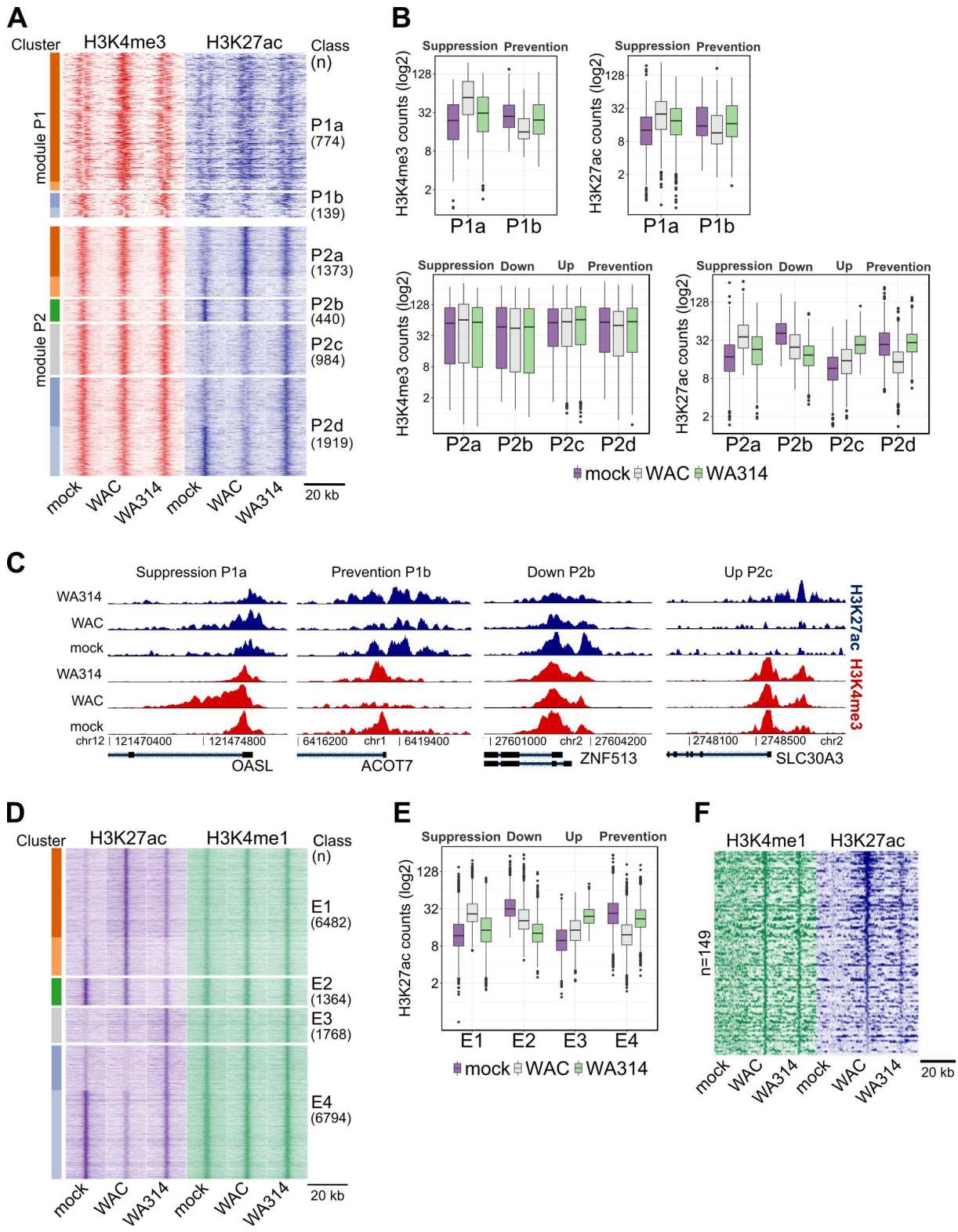

Fig 2. Dynamic chromatin modifications at promoters and enhancers in *Y. enterocolitica* infected macrophages.

A, Heatmap showing clustering of all H3K4me3 (module P1) and H3K27ac (module P2) differentially enriched regions at promoters in mock-, WAC- and WA314 infected human

1422 macrophages. P1 contains dynamic H3K4me3 regions and P2 contains dynamic H3K27ac
1423 regions at largely constant H3K4me3 regions. H3K4me3 and H3K27ac tag densities are
1424 shown in both modules. The identified clusters (colour coded bars on the left side) were
1425 grouped in classes P1a-P2d.
1426 **B,** Boxplots of H3K4me3 and H3K27ac tag counts for the classes in **(A)**. Profiles describing
1427 relation of histone mark levels between mock, WAC and WA314 are indicated on top. Data
1428 are representative of at least two independent experiments.
1429 **C** Peak tracks of H3K4me3 (red) and H3K27ac (blue) ChIP-seq tag densities at promoter
1430 regions of the genes OASL from Suppression profile classes P1a and ACOT7 from Prevention
1431 profile class P1b (left) and ZNF513 from Down profile class P2b and SLC30A3 from Up profile
1432 class P2c (right).
1433 **D,** Heatmap showing clustering of H3K27ac differentially enriched regions at enhancers of
1434 mock-, WAC- and WA314 infected macrophages. H3K4me1 tag counts are shown for the
1435 associated regions. Clustering analysis yielded 6 clusters (color coded, left side) which were
1436 assembled into classes E1-4.
1437 **E,** Boxplot of H3K27ac tag counts of classes E1-E4 in **(D)**. Profiles describing relation of
1438 histone mark levels between mock, WAC and WA314 are indicated on top. Data are
1439 representative of two independent experiments.
1440 **F,** Heatmap showing H3K4me1 and H3K27ac tag counts at latent enhancers induced by WAC
1441 vs mock. For **(A)**, **(D)** and **(F)** rows are genomic regions from -10 to +10 kb around the centre
1442 of the analyzed regions. “n” indicates number of regions.
1443
1444

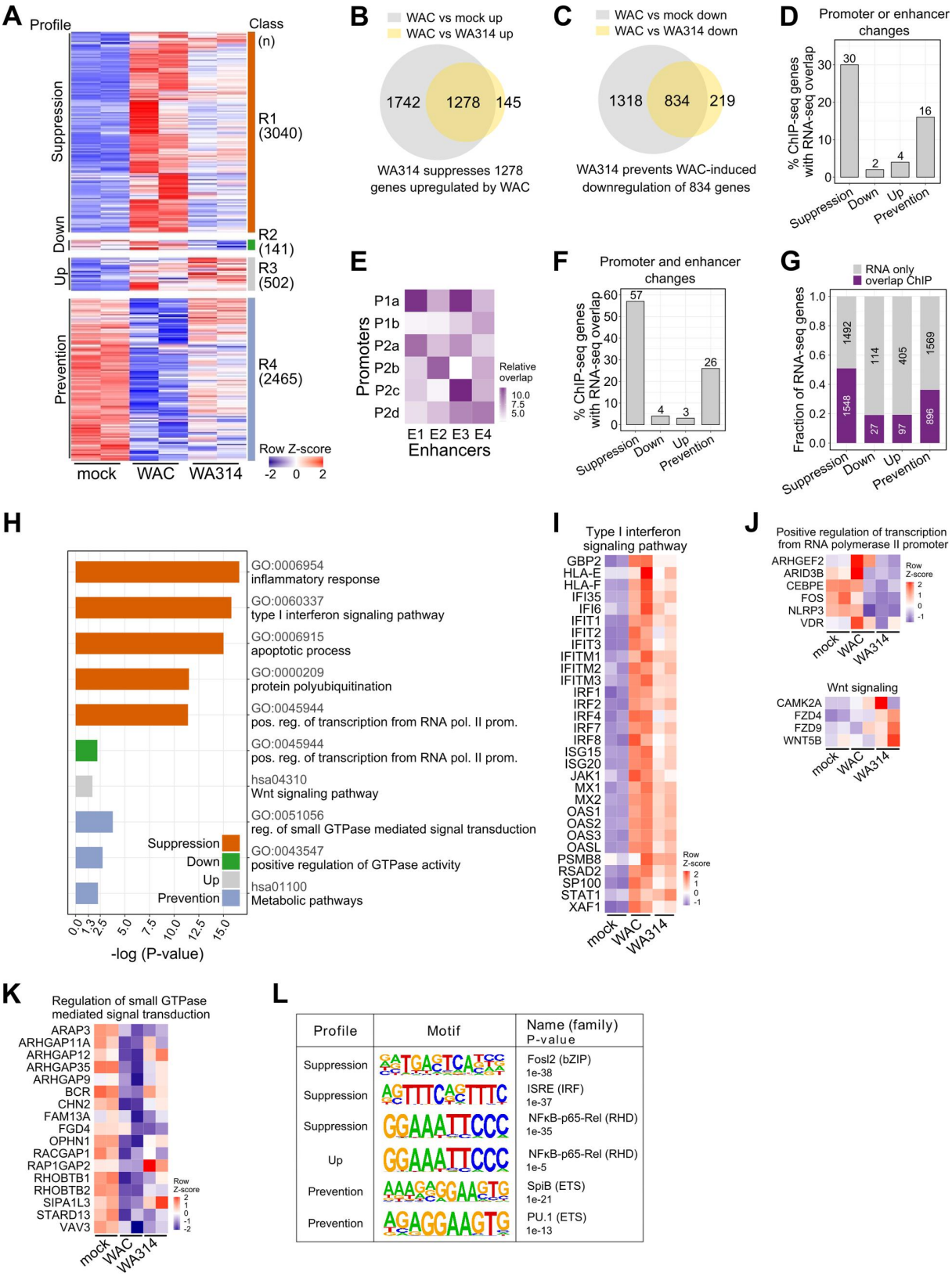

Fig 3. Association between histone modifications and gene expression in *Y. enterocolitica* infected macrophages.

1448 **A,** Heatmap from clustering of all DEGs from mock, WAC and WA314 comparisons.
1449 Clustering identified 4 major classes R1-R4 (color coded, right side). Profiles describing
1450 relation of expression levels between mock, WAC and WA314 are indicated on the left. In
1451 the heatmap, gene rlog counts are row-scaled (row Z-score).
1452 **B, C,** Venn diagrams of DEG overlaps between WAC vs mock up and WAC vs WA314 up **(B)**
1453 and WAC vs mock down and WAC vs WA314 down **(C)**. Overlaps show the number of genes
1454 whose up-regulation by WAC is suppressed by WA314 **(B)** and whose down-regulation by
1455 WAC is prevented by WA314 **(C)**.
1456 **D,** Barplot showing percentage of genes from ChIP-seq profiles with promoter or enhancer
1457 modifications overlapping with corresponding RNA-seq profiles from DEG analysis.
1458 **E,** Heatmap presentation showing relative overlap of genes in promoter classes P1a-P2d and
1459 enhancer classes E1-4. Light to dark color scale indicates low to high overlap.
1460 **F,** Barplot showing percentage of genes with coordinated promoter and enhancer changes
1461 from ChIP-seq profiles in **(E)** overlapping with corresponding RNA-seq profiles.
1462 **G,** Bar plot showing fraction and number (numbers in bars) of genes from RNA-seq profiles
1463 overlapping with genes from corresponding ChIP-seq profiles at promoters or enhancers.
1464 **H,** Bar plot showing enriched GO and KEGG (hsa prefix) terms for genes overlapping in RNA-
1465 seq and ChIP-seq as in **(G)**. Bars represent log10 transformed P-values correlating with
1466 significance of enrichment. Pos: positive, reg: regulation, pol: polymerase, prom: promoter.
1467 **I-K,** Heatmaps of row-scaled (row Z-score) RNA-seq rlog gene counts for genes with RNA-seq
1468 and ChIP-seq promoter or enhancer overlaps from pathways in **(H)**.
1469 **J,** Representative enriched transcription factor motifs in promoter and enhancer regions of
1470 genes with RNA-seq and ChIP-seq (promoter or enhancer) overlaps as in **(G)**.
1471

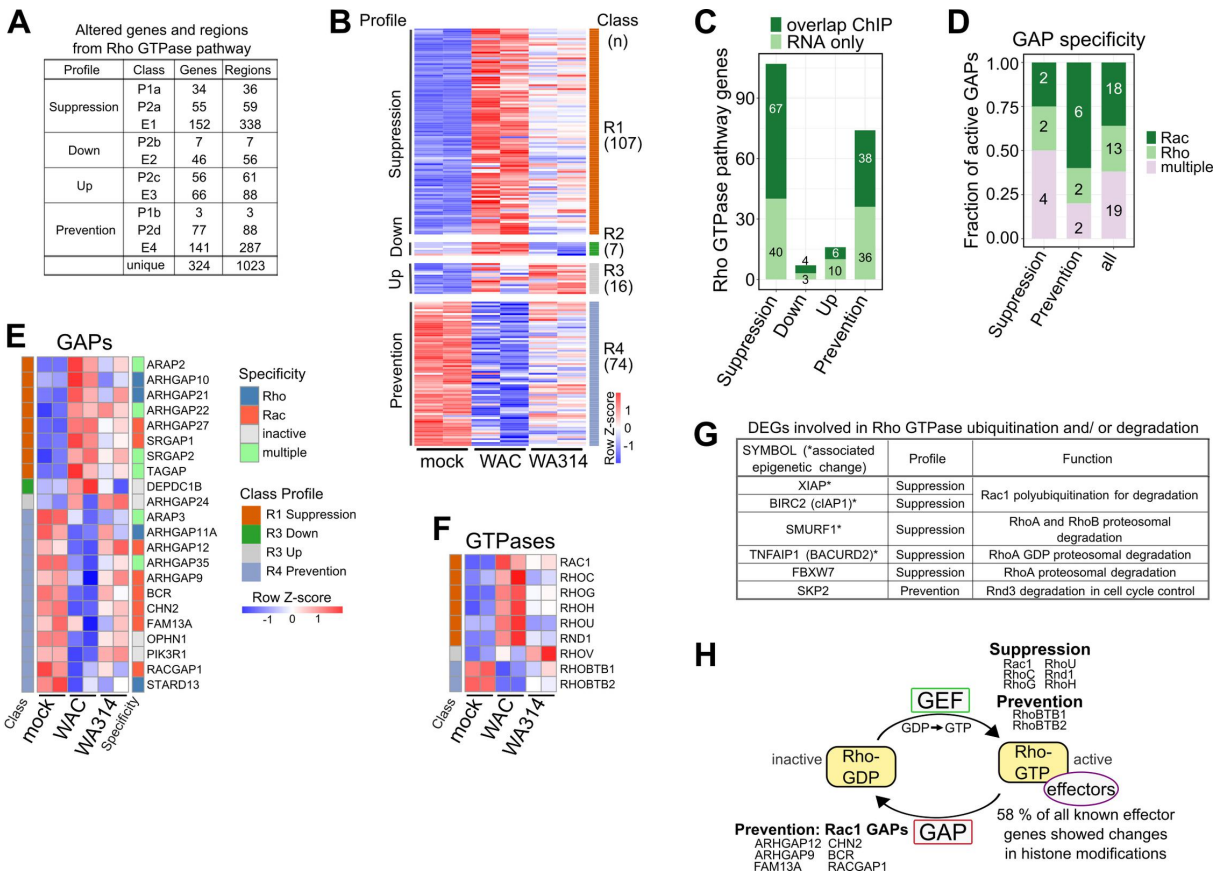

Fig 4. Epigenetic and transcriptional regulation of Rho GTPase pathway genes in *Y. enterocolitica* infected macrophages.

A, Number of Rho GTPase pathway genes associated with changed regions in promoter (P1-b, P2a-d) or enhancer (E1-4) classes. "Unique" refers to total unique genes or regions (overlapping regions were merged together) when counting together all promoter and enhancer classes.

B, Heatmap of all DEGs from Rho GTPase pathway belonging to classes R1-R4 (color coded, right side) in Fig 3A. Association with profiles is shown on the left side. "n" refers to the number of genes. Gene rlog counts were row-scaled (row Z-score).

C, Bar plot showing number of DEGs belonging to Rho GTPase pathway from RNA-seq profiles in **(B)** overlapping with genes with corresponding promoter (P1a-b, P2a-d classes) and/ or enhancer (E1-4 classes) changes from the same profiles.

1485 **D,** Bar plot showing Rho GTPase specificity of active GAPs (Müller et al., 2020) for genes with
1486 RNA-seq and ChIP-seq overlaps in **(C).**.Fraction and number (in bars) for all active GAPs and
1487 for GAPs in the Suppression and Prevention profiles are shown.
1488 **E, F,** Heatmaps of RNA-seq rlog counts for GAP **(E)** and Rho GTPase genes **(F)** with RNA-seq
1489 and ChIP-seq overlaps in **(C)**. Associated profiles are indicated on the left and specificity of
1490 GAPs for Rho GTPases are indicated on the right. Gene rlog counts were row-scaled (row Z-
1491 score).
1492 **G,**Table showing DEGs (from Fig 3A, S6 Table) known to regulate ubiquitination and/ or
1493 proteosomal degradation of Rho GTPases.
1494 **H,** Schematic representation of Rho GTPase cycle showing reprogrammed Rho GTPase
1495 pathway genes divided into GAPs, GEFs, Rho GTPases and effectors, and assigned to profiles.
1496
1497

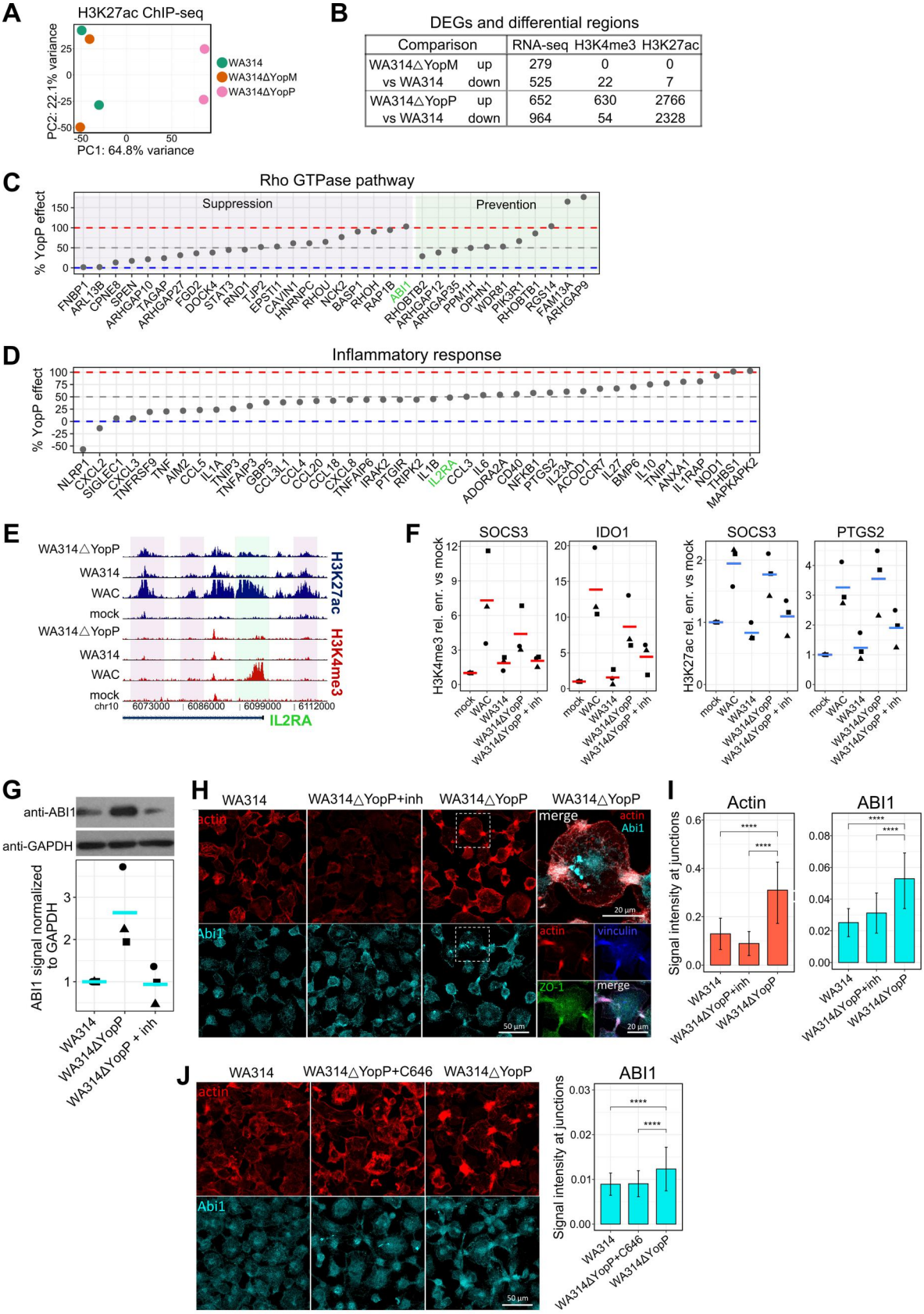

Fig 5. Role of YopP and YopM in the epigenetic and transcriptional reprogramming of macrophages by *Y. enterocolitica*.

1501 **A,** Principal component analysis of H3K27ac tag counts in classes P1a-P2d and E1-4 in two
1502 replicates of macrophages infected with the indicated strains.
1503 **B,** Number of statistically significant (≥ 2-fold change, adjusted P-value ≤ 0.05) DEGs and
1504 differentially enriched H3K4me3 and H3K27ac regions for WA314ΔYopM vs WA314 and
1505 WA314ΔYopP vs WA314.
1506 **C, D,** Percentage of WA314 effect on expression of Rho GTPase pathway **(C)** or Inflammatory
1507 response **(D)** genes that is caused by YopP. Genes with associated promoter or enhancer
1508 changes from the same profile and significant change for RNA-seq (DESeq2) and ChIP-seq
1509 (diffReps) between WAC vs WA314 are shown. The percentage value was calculated from
1510 the ratio of fold change (FC) between WA314ΔYopP vs WA314 and WA314 vs WAC for
1511 Suppression **(C, D)** and Prevention **(C)** profiles.
1512 **E,** Peak tracks of ChIP-seq tag densities showing H3K4me3 and H3K27ac changes associated
1513 with IL2RA gene, whose suppression of gene expression by WA314 is produced in a YopP-
1514 dependent manner **(D)**. H3K4me3 and H3K27ac densities at the IL2RA promoter (green
1515 shade) and H3K27ac densities at the enhancers (purple shade) are not affected by YopP
1516 (compare effects of WA314 and WA314ΔYopP).
1517 **F,** Dot plots of H3K4me3 and H3K27ac ChIP-qPCR signals at indicated genes in macrophages
1518 not infected (mock) or infected with indicated strains. WA314ΔYopP infections occurred in
1519 the absence and presence of MAPK inhibitors (inh). The ChIP-qPCR signal was expressed as
1520 relative (rel.) enrichment (enr.) vs mock. Lines represent mean of 3 biological replicates (dots
1521 with different shapes). SOCS3: Suppressor of cytokine signaling 3, IDO1: Indoleamine 2,3-
1522 Dioxygenase 1, PTGS2: Prostaglandin-Endoperoxide Synthase 2.
1523 **G,** Western blot analysis (top) and quantification (bottom) of ABI1 levels in primary human
1524 macrophages infected with WA314, WA314ΔYopP and WA314ΔYopP+inh (MAPK inhibitors)

1525 at an MOI of 100 for 6 h. GAPDH was used as a loading control and for normalization of ABI1
1526 signal. Western blot is representative of three independent experiments shown in
1527 quantification.
1528 **H,** Immunofluorescence staining of primary human macrophages infected with WA314,
1529 WA314ΔYopP+inh (MAPK inhibitors) and WA314ΔYopP with MOI of 100 for 6 h. Cells were
1530 stained with Alexa568 phalloidin (red) to visualize actin and antibodies for ABI1 (cyan),
1531 vinculin (blue) and ZO-1 (green). Fourth column shows an overlay of actin and ABI1 (top) and
1532 actin, vinculin and ZO-1 (bottom) for WA314ΔYopP infection. Data are representative of two
1533 independent experiments.
1534 **I,** Quantification of actin (left) and ABI1 (right) signal intensity at cell junctions from
1535 immunofluorescence of primary human macrophages infected with WA314,
1536 WA314ΔYopP+inh (MAPK inhibitors) and WA314ΔYopP with MOI of 100 for 6 h. Data are
1537 representative of two independent experiments.
1538 **J,** Immunofluorescence staining of primary human macrophages infected with WA314,
1539 WA314ΔYopP+C646 (p300 inhibitor) and WA314ΔYopP with MOI of 100 for 6 h (left). Cells
1540 were stained with Alexa568 phalloidin (red) to visualize actin and antibody for ABI1 (cyan).
1541 Quantification of ABI1 signal at cell cell contacts is shown on the right. Data are
1542 representative of two independent experiments. In **(I)** and **(J)** bars show mean and error bars
1543 represent standard deviation. ****: P-adjusted < 0.0001 by unpaired Wilcoxon test.
1544
1545
1546

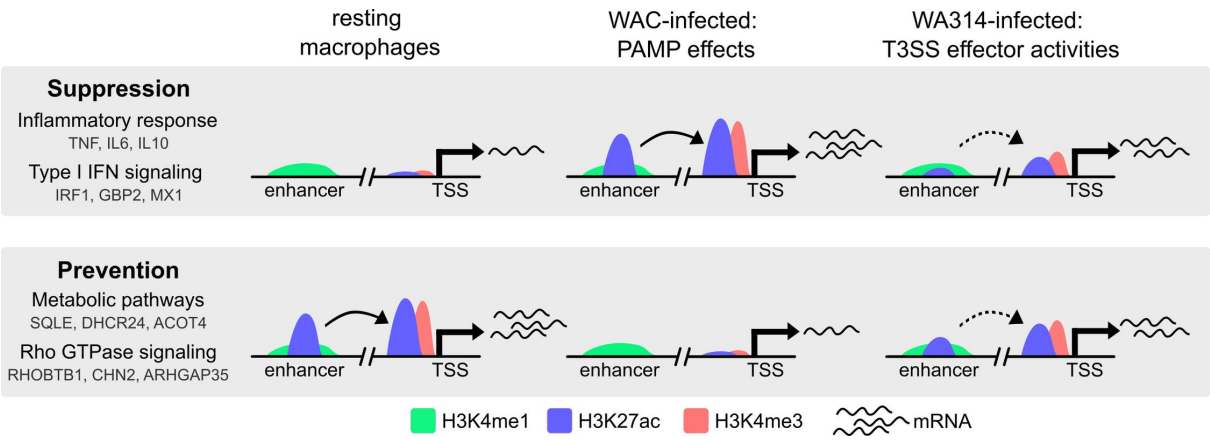

Fig 6. Summary schematic showing the main effects of *Y. enterocolitica* on macrophage chromatin in gene expression. Plasmid-encoded virulence factors suppress upregulation (Suppression profile) and prevent downregulation (Prevention profile) of PAMP induced H3K27ac and H3K4me3 changes at gene promoters and/ or enhancers and consequently the expression of associated genes. Suppression profile is associated with genes from Inflammatory response and Type I IFN signaling, whereas Prevention profile is associated with genes from Metabolic pathways and Rho GTPase signaling. Representative genes belonging to each pathway are shown. Enhancer activity is indicated with arched arrows. Increased promoter activity is indicated with more mRNAs.

Supporting information

Figures

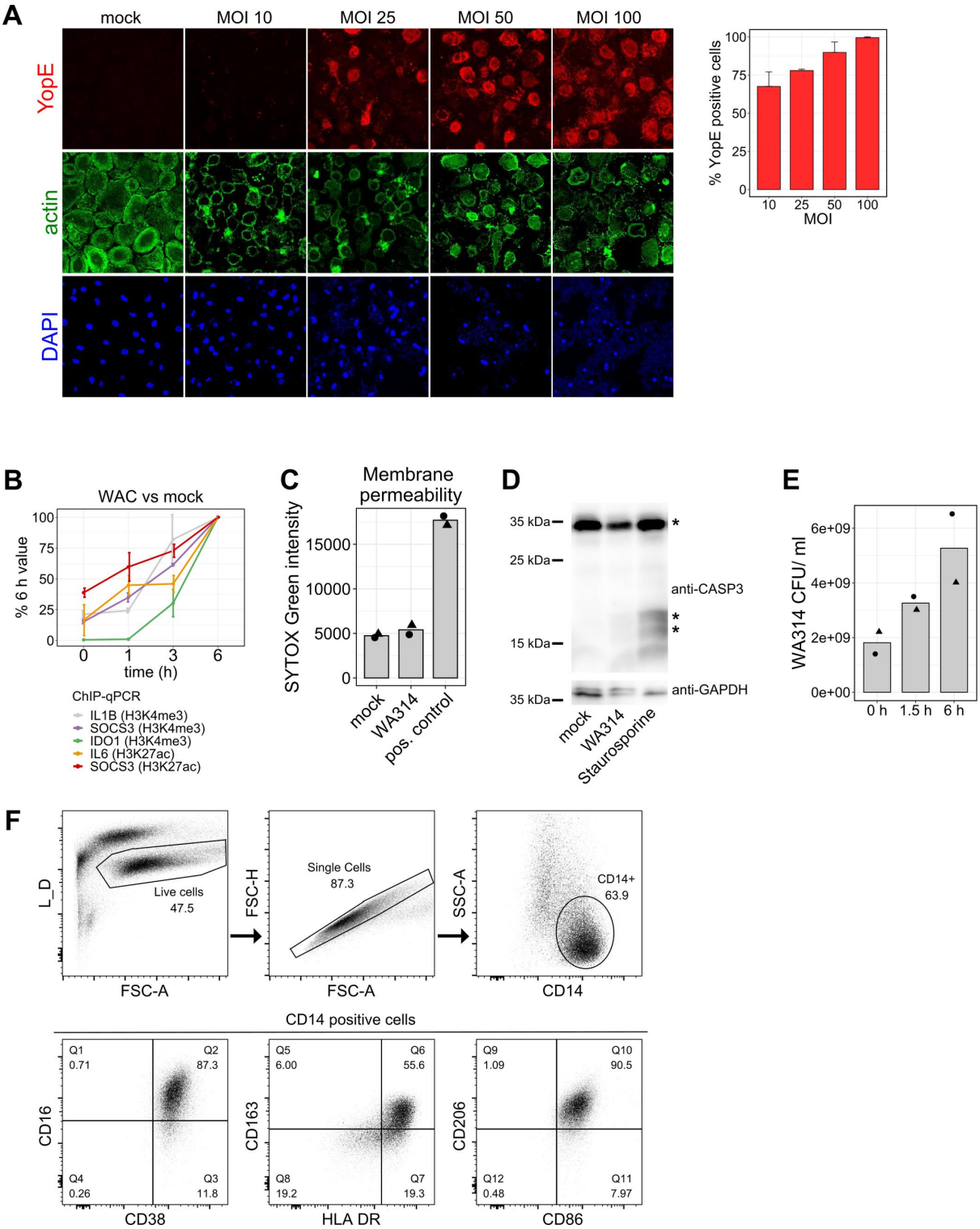

Fig S1. Analysis of infection conditions.

1562 **A,** Left: Immunofluorescence staining of primary human macrophages mock infected or
1563 infected with WA314-YopE-ALFA for 6 h with MOI 10, 25, 50 or 100. Cells were stained with
1564 anti-ALFA nanobody-635 (red) to visualize YopE, Alexa568 phalloidin (green) to visualize actin
1565 and DAPI (blue) to visualize nucleus. Right: Quantification of YopE-ALFA positive cells. Bars
1566 show mean and error bars represent standard deviation when analyzing two different
1567 coverslips.
1568 **B,** Line plot showing time course H3K4me3 (IL1B, SOCS3, IDO1 genes) and H3K27ac (IL6,
1569 SOCS3 genes) ChIP-qPCR analysis of WAC infected primary human macrophages with MOI of
1570 100. Lines represent means and error bars represent standard deviation from two
1571 independent macrophage donors/ biological replicates.
1572 **C,** Bar plot showing membrane permeability due to cell death in primary human
1573 macrophages mock infected, infected with WA314 (MOI of 100) or treated with positive
1574 (pos.) control (1 % TRITON-X-100) for 6 h. Increased membrane permeability is expressed as
1575 higher SYTOX Green intensity, where the dye binds to DNA and emits fluorescence when
1576 plasma membrane integrity is compromised. Bars represent means of two biological
1577 replicates/ macrophage donors (dots with different shapes).
1578 **D,** Western blot analysis of primary human macrophages showing caspase-3 cleavage in
1579 mock or WA314 (MOI 100) infected cells or treated with positive control Staurosporine (5
1580 µM) for 6 h. * indicates full length caspase-3 (35 kDa) and cleavage fragments (17 and 19
1581 kDa). GAPDH was used as a loading control. Data are representative of four biological
1582 replicates/ different macrophage donors.
1583 **E,** Bar plot showing colony forming unit (CFU) analysis of *Y. enterocolitica* WA314 growth
1584 during infection of primary human macrophages for 0 h, 1.5 h or 6 h at 37 °C. Bars represent
1585 means of two different biological replicates (dots with different shapes).

1586 **F,** Flow cytometry analysis of monocyte-derived primary human macrophages after 6 days of
1587 differentiation. Live cells (L/D negative) were selected (blue areas; first top panel) and
1588 doublets excluded (second top panel). CD14 positive macrophages were selected (third top
1589 panel) and analyzed for expression of macrophage markers CD163, CD38, CD86, HLA-
1590 DR,CD206 and CD16 (bottom panels).
1591
1592
1593

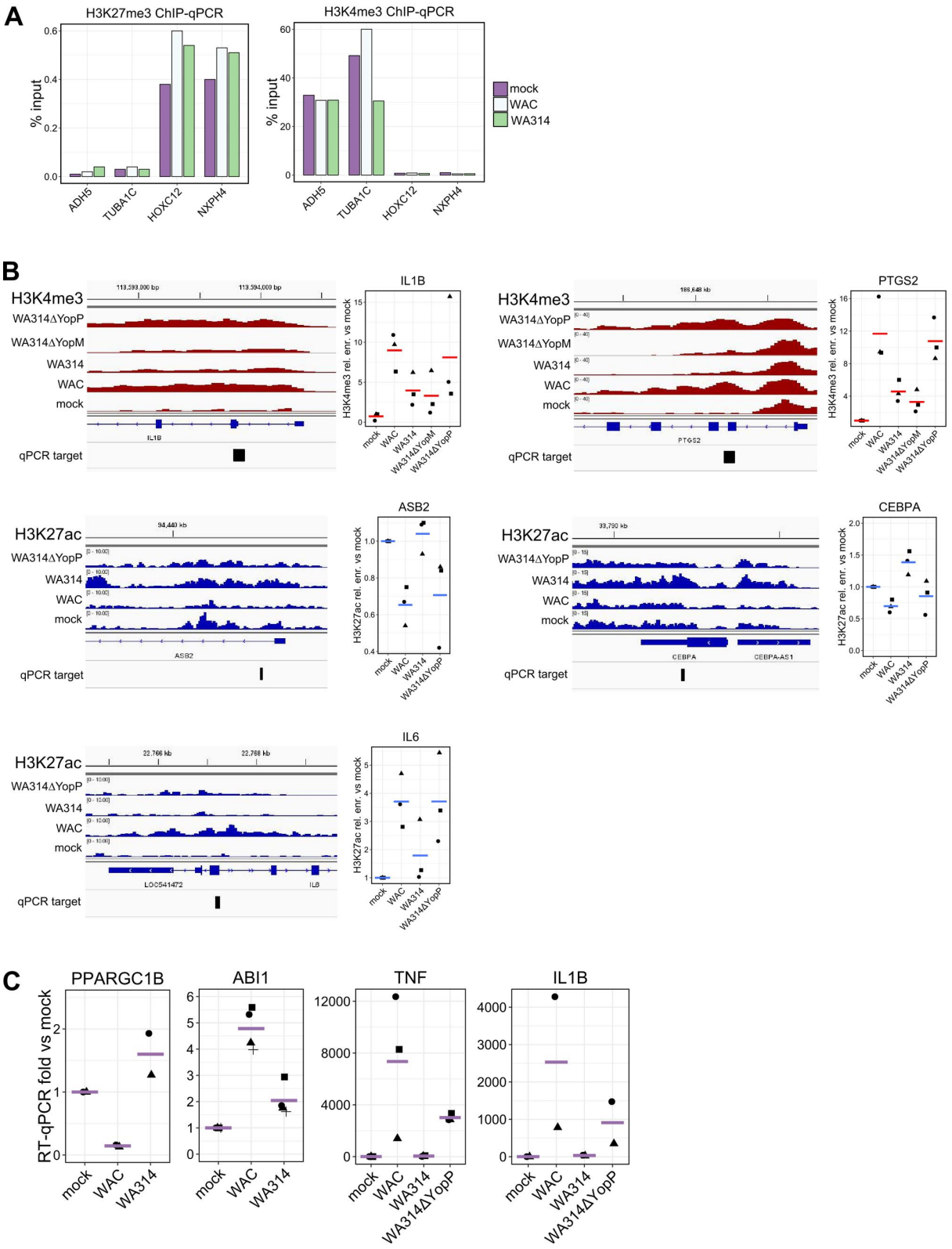

Fig S2. Confirmation of ChIP-seq and RNA-seq results by qPCR.

A, Bar plot showing H3K27me3 (left) and H4K4me3 (right) ChIP-qPCR from primary human macrophages mock infected or infected with WAC or WA314 for 6 h with MOI of 100. HOXC12 and NXPH4 are positive controls for H3K27me3 and ADH5 and TUBA1C are positive

1599 controls for H3K4me3. Data are representative of at least two experiments with different
1600 biological replicates/ macrophage donors.
1601 **B,** Peak tracks showing tag density of H3K4me3 (red) or H3K27ac (blue) ChIP-seq from
1602 primary human macrophages infected for 6 h with indicated strains (MOI of 100) (left). qPCR
1603 target refers to the primer binding site used for fragment amplification in ChIP-qPCR analysis
1604 shown as a dot plot (right). The ChIP-qPCR signal was expressed as relative (rel.) enrichment
1605 (enr.) vs mock. Lines represent means from at least two different biological replicates/
1606 macrophage donors (dots with different shapes).
1607 **C,** Dot plots showing gene expression analysis of PPARGC1B, ABI1, TNF and IL1B genes with
1608 RT-qPCR from primary human macrophages infected for 6 h with indicated strains (MOI 100).
1609 The RT-qPCR signal was expressed as fold vs mock. Lines represent means from at least two
1610 different biological replicates/ macrophage donors (dots with different shapes).
1611
1612

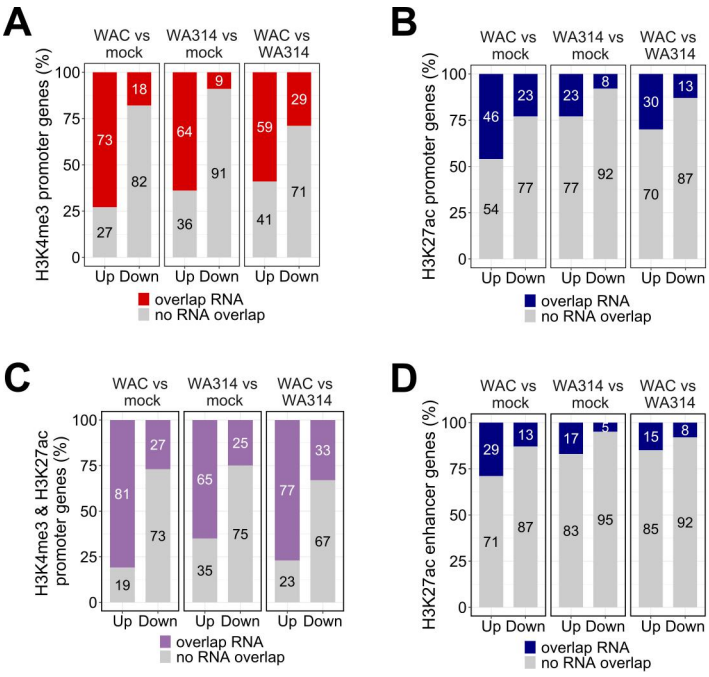

Fig S3. Analysis of association between histone marks and gene expression.

A-D, Bar plots showing fraction (%) of genes associated with H3K4me3 at promoter **(A)**, H3K27ac at promoter **(B)**, H3K4me3 and H3K27ac at promoter **(C)** and H3K27ac at enhancer **(D)** changes for comparisons between mock, WAC and WA314 showing significant (≥ 2-fold change, adjusted P-value ≤ 0.05) associated change in gene expression (overlap RNA).

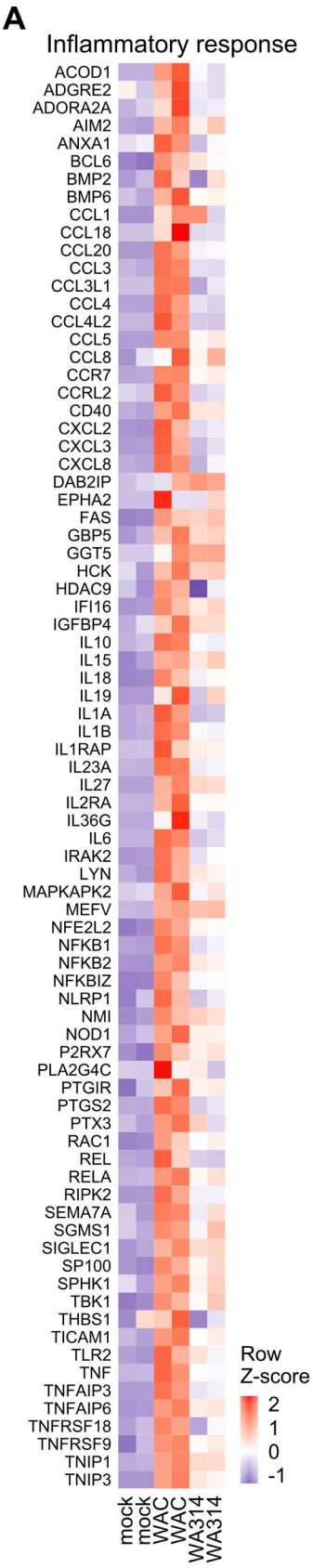

B

GO terms associated with latent enhancers

Term	P-value	Genes
GO:0000122~negative regulation of transcription from RNA polymerase II promoter	1.13E-04	ATF7IP, SP100, EDN1, BCL11A, NEDD4L, RBPJ, NFKB1, FOXP1, ZEB2, REST, H2AFY2, REL, PKIG, JARID2, EZH2
GO:0006954~inflammatory response	0.0022	SP100, TNFAIP6, IL2RA, CCL3L3, REL, TNFAIP3, IL19, CCR7, NFKB1

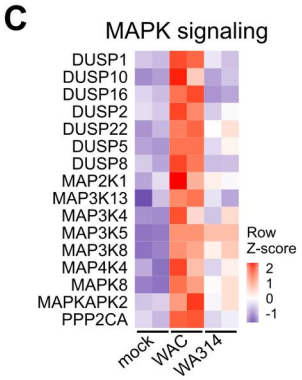

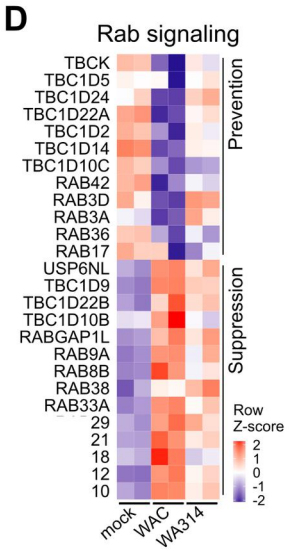

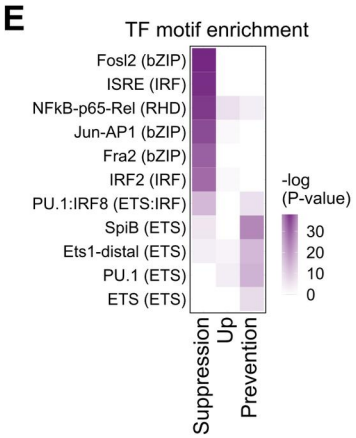

1621

1622 **Fig S4. Pathway and transcription factor motif enrichment analysis of genes with**
1623 **associated histone modification and gene expression changes during *Y. enterocolitica***
1624 **infection.**
1625 **A,** Heatmap of row-scaled (row Z-score) RNA-seq rlog gene counts for genes with RNA-seq
1626 and ChIP-seq promoter or enhancer overlaps belonging to "Inflammatory response"
1627 pathway as in Figure 3H.
1628 **B,** GO terms associated with latent enhancer genes from Figure 2F.
1629 **C-D,** Heatmaps of row-scaled (row Z-score) RNA-seq rlog gene counts for selected genes with
1630 RNA-seq and ChIP-seq promoter or enhancer overlaps belonging to phosphatases and
1631 kinases from MAPK signalling in Suppression profile **(C)** and Rab GTPase pathway in
1632 Prevention and Suppression profiles **(D)** from S16 Table.
1633 **E,** Heatmap showing transcription factor motif enrichment in promoter and enhancer
1634 regions of genes with RNA-seq and ChIP-seq overlaps from Figure 3G. Color indicates level of
1635 log10 transformed P-value positively correlating with significance of enrichment.
1636
1637

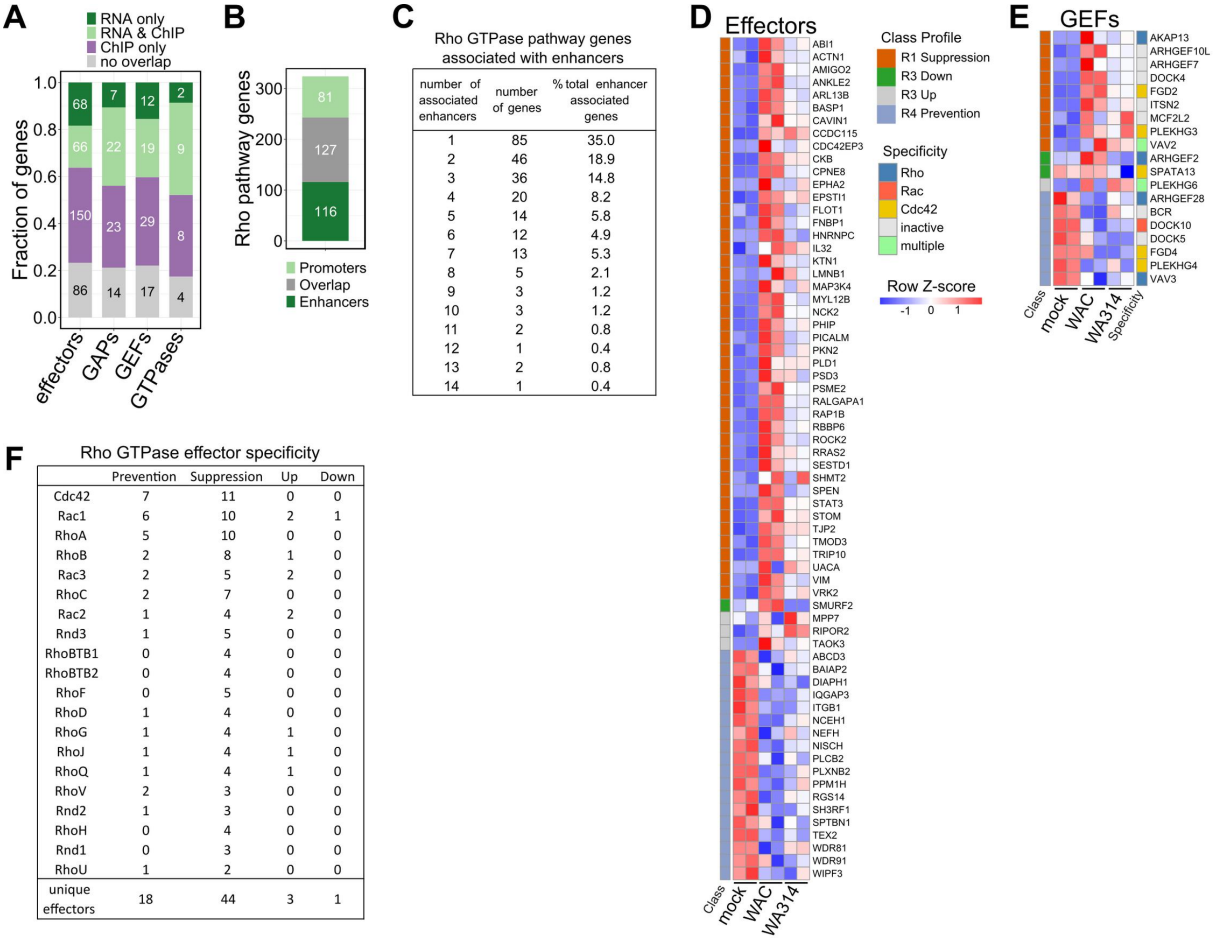

number of associated enhancers	number of genes	% total enhancer associated genes
1	85	35.0
2	46	18.9
3	36	14.8
4	20	8.2
5	14	5.8
6	12	4.9
7	13	5.3
8	5	2.1
9	3	1.2
10	3	1.2
11	2	0.8
12	1	0.4
13	2	0.8
14	1	0.4

	Prevention	Suppression	Up	Down
Cdc42	7	11	0	0
Rac1	6	10	2	1
RhoA	5	10	0	0
RhoB	2	8	1	0
Rac3	2	5	2	0
RhoC	2	7	0	0
Rac2	1	4	2	0
Rnd3	1	5	0	0
RhoBTB1	0	4	0	0
RhoBTB2	0	4	0	0
RhoF	0	5	0	0
RhoD	1	4	0	0
RhoG	1	4	1	0
RhoJ	1	4	1	0
RhoQ	1	4	1	0
RhoV	2	3	0	0
Rnd2	1	3	0	0
RhoH	0	4	0	0
Rnd1	0	3	0	0
RhoU	1	2	0	0
unique effectors	18	44	3	1

Fig S5. Epigenetic and transcriptional regulation of Rho GTPase pathway genes in *Y. enterocolitica* infected macrophages.

A, Bar plot showing fraction and number (in bars) of indicated Rho GTPase pathway genes with changes in expression only (RNA only), any associated histone modification only (ChIP only), overlaps between RNA-seq and ChIP-seq (RNA & ChIP) and no overlap with neither ChIP-seq nor RNA-seq (no overlap).

B, Bar plot showing number of Rho GTPase pathway genes with dynamic histone modifications at promoters, enhancers or both (overlap).

C, Table showing number of Rho GTPase pathway genes with histone modification changes at enhancers and number of associated enhancers. “% total enhancer associated genes” indicates what fraction of all Rho GTPase pathway genes with changes at enhancers show a certain number of changed enhancers.

1651 **D, E,** Heatmaps of DEGs with associated histone modification changes at promoters or

1652 enhancers encoding Rho GTPase effectors **(D)** and GEFs **(E)** . Associated profiles are color

1653 coded on the left. The specificity of GEFs for Rho GTPases is color coded on the right **(E)**.

1654 Gene rlog counts were row-scaled (row Z-score).

1655 **F,** Table showing specificity of Rho GTPase effectors associated with RNA-seq and ChIP-seq

1656 overlaps in **(A)** and Figure 4C.

1657

1658

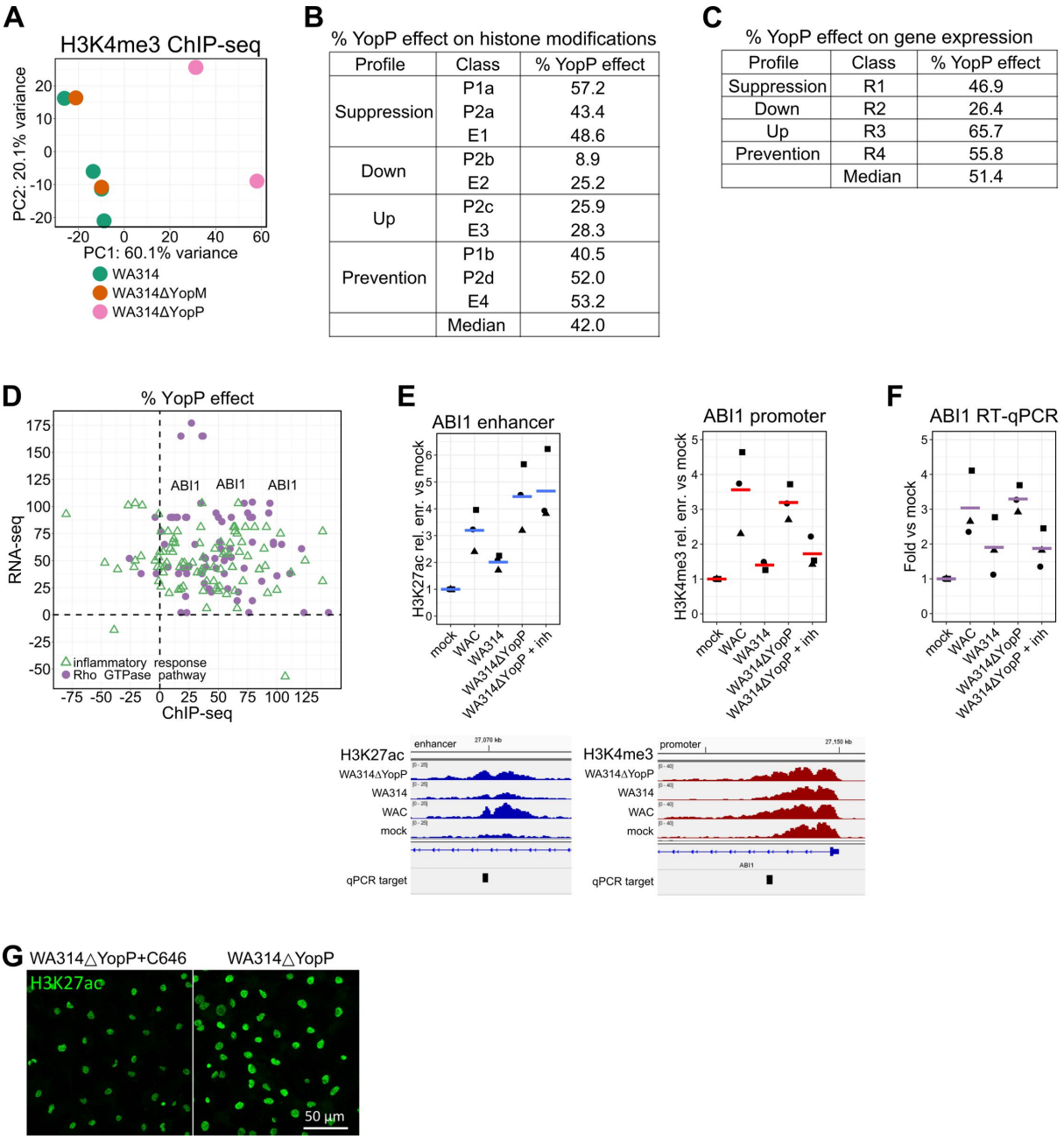

Profile	Class	% YopP effect
Suppression	P1a	57.2
	P2a	43.4
	E1	48.6
Down	P2b	8.9
	E2	25.2
Up	P2c	25.9
	E3	28.3
Prevention	P1b	40.5
	P2d	52.0
	E4	53.2
	Median	42.0

Profile	Class	% YopP effect
Suppression	R1	46.9
Down	R2	26.4
Up	R3	65.7
Prevention	R4	55.8
	Median	51.4

Fig S6. Analysis of YopM and YopP effect on epigenetic and gene expression changes in macrophages upon *Y. enterocolitica* infection.

A, Principal component analysis of H3K4me3 tag counts in classes P1a-b of macrophages infected with the indicated strains for all biological replicates used in the analysis.

B, Percentage YopP effect (median value) for H3K4me3 (P1a-b classes) and H3K27ac (P2a-d, E1-4 classes) when compared to WA314 vs mock (Up and Down profiles) or WA314 vs WAC (Suppression and Prevention profiles)**.**

1667 **C,** Percentage YopP effect (median value) for DEGs associated with respective histone
1668 modification changes at promoters or enhancers. “Median”: median value when taking %
1669 YopP effect from all classes together.
1670 **D,** Scatter plot of % YopP effect for RNA-seq DEGs and ChIP-seq differential regions for genes
1671 with associated gene expression and histone modification change from Rho GTPase and
1672 Inflammatory response pathways from Figures 5C, D. Purple dots associated with ABI1 gene
1673 are indicated.
1674 **E,** Top: Dot plots showing ChIP-qPCR of H3K27ac at enhancer within ABI1 gene and
1675 H3K4me3 at ABI1 promoter from primary human macrophages infected for 6 h with
1676 indicated strains (MOI of 100)**.** Lines represent means from three different biological
1677 replicates/ macrophage donors (dots with different shapes). Bottom: Peak tracks showing
1678 tag density of H3K27ac at enhancer (blue) and H3K4me3 at promoter (red) ChIP-seq and
1679 primer binding site used for fragment amplification in ChIP-qPCR analysis (qPCR target)
1680 shown in dot plots. The ChIP-qPCR signal was expressed as relative (rel.) enrichment (enr.) vs
1681 mock. inh: MAPK inhibitors.
1682 **F,** Dot plots showing RT-qPCR gene expression analysis of ABI1 from primary human
1683 macrophages infected for 6 h with indicated strains (MOI of 100). The RT-qPCR signal was
1684 expressed as fold vs mock. Lines represent means from three different biological replicates/
1685 macrophage donors (dots with different shapes). inh: MAPK inhibitors.
1686 **G,** Immunofluorescence staining of primary human macrophages infected with
1687 WA314ΔYopP+C646 (p300 inhibitor) and WA314ΔYopP with MOI of 100 for 6 h. Cells were
1688 stained with antibody for H3K27ac. Images are representative of two independent
1689 experiments.
1690

1691 # Tables

1692 **S1 Table. *Yersinia enterocolitica* strains used in the study.**

1693 **S2 Table. Analysis of promoter regions in P1 and P2 modules.**

1694 **S3 Table. Analysis of enhancer regions in E1-4 classes.**

1695 **S4 Table. Analysis of latent enhancers.**

1696 **S5 Table. RNA-seq background from DESeq2 analysis.**

1697 **S6 Table. Clustering of RNA-seq DEGs in a heatmap.**

1698 **Table S7. Metabolic pathways in Prevention profile.**

1699 **S8 Table. Enriched pathways associated with Rho GTPase pathway genes.**

1700 **S9 Table. Analysis of Rho GTPase pathway genes in promoter and enhancer classes.**

1701 **S10 Table. RNA-seq heatmap of DEGs from Rho GTPase pathway.**

1702 **S11 Table. Rho GTPase specificity of GAPs and GEFs with RNA-seq and ChIP-seq overlaps in**

1703 **different profiles.**

1704 **S12 Table. Rho GTPase specificity and reported function in epigenetics for effectors with**

1705 **RNA-seq and ChIP-seq overlaps.**

1706 **S13 Table. Analysis of YopP effect on Rho GTPase pathway genes.**

1707 **S14 Table. Analysis of YopP effect on inflammatory response pathway genes.**

1708 **S15 Table. Primer sequences used for ChIP-qPCR and RT-qPCR analysis.**

1709 **S16 Table. Enriched pathways associated with trafficking, MAPK signaling, Akt signaling**

1710 **and cell death.**

1711 **S17 Table. Summary of all replicates used for ChIP-seq and RNA-seq experiments.**

1712 **S18 Table. All filtered differentially enriched regions for histone marks based on diffReps**

1713 **analysis.**

1714